


Mutation of the 3-Phosphoinositide-Dependent Protein Kinase 1 (PDK1) Substrate-Docking Site in the Developing Brain Causes Microcephaly with Abnormal Brain Morphogenesis Independently of Akt, Leading to Impaired Cognition and Disruptive Behaviors

Lluís Cordón-Barris,^{a*} Sònia Pascual-Guiral,^a Shaobin Yang,^a Lydia Giménez-Llort,^b Silvia Lope-Piedrafitra,^c Carlota Niemeyer,^a Enrique Claro,^a Jose M. Lizcano,^a  Jose R. Bayascas^a

Institut de Neurociències and Departament de Bioquímica i Biologia Molecular, Unitat de Bioquímica de Medicina, Universitat Autònoma de Barcelona, Barcelona, Spain^a; Institut de Neurociències and Departament de Psiquiatria i Medicina Legal, Universitat Autònoma de Barcelona, Barcelona, Spain^b; Servei de Resonància Magnètica Nuclear, Universitat Autònoma de Barcelona, and Centro de Investigación Biomédica en Red en Bioingeniería, Biomateriales y Nanomedicina (CIBER-BBN), Barcelona, Spain^c

The phosphoinositide (PI) 3-kinase/Akt signaling pathway plays essential roles during neuronal development. 3-Phosphoinositide-dependent protein kinase 1 (PDK1) coordinates the PI 3-kinase signals by activating 23 kinases of the AGC family, including Akt. Phosphorylation of a conserved docking site in the substrate is a requisite for PDK1 to recognize, phosphorylate, and activate most of these kinases, with the exception of Akt. We exploited this differential mechanism of regulation by generating neuron-specific conditional knock-in mice expressing a mutant form of PDK1, L155E, in which the substrate-docking site binding motif, termed the PIF pocket, was disrupted. As a consequence, activation of all the PDK1 substrates tested except Akt was abolished. The mice exhibited microcephaly, altered cortical layering, and reduced circuitry, leading to cognitive deficits and exacerbated disruptive behavior combined with diminished motivation. The abnormal patterning of the adult brain arises from the reduced ability of the embryonic neurons to polarize and extend their axons, highlighting the essential roles that the PDK1 signaling beyond Akt plays in mediating the neuronal responses that regulate brain development.

The phosphoinositide 3-kinase (PI3K) signaling pathway regulates cell survival, proliferation, growth, and motility, as well as metabolism, in response to extracellular signals. Class I PI3Ks phosphorylate the membrane phospholipid phosphatidylinositol-4,5-bisphosphate [PtdIns(4,5)P₂] to generate the phosphatidylinositol-3,4,5-trisphosphate [PtdIns(3,4,5)P₃] second messenger (1, 2). In neurons, stimulation of PI3K by neurotrophic factors, neurotransmitters, or guidance cues results in the activation of protein kinase B (PKB) (also termed Akt), the most studied downstream effector of this signaling pathway. Akt phosphorylates and inactivates a number of cellular substrates controlling different aspects of neuronal development. They include PRAS40 and TSC2, leading to mammalian TORC1 (mTORC1) activation, which in turn promotes the synthesis of selected sets of proteins involved in the differentiation program (3); glycogen synthase kinase 3 (GSK3), which regulates cytoskeleton dynamics and participates in the establishment and maintenance of neuronal polarity (4, 5); and FOXO, which promotes the expression of genes inhibiting apoptosis (6). Genetic analysis in mice has uncovered the functional significance of PI3K for brain morphology and physiology (7–10), whereas deregulation of this signaling pathway has pathophysiological consequences in human neurodevelopmental disorders, such as schizophrenia (11–13) and autism (14, 15).

3-Phosphoinositide-dependent protein kinase 1 (PDK1) transduces many agonist-induced cellular responses by activating an entire set of AGC kinase family members, in addition to Akt (16). They include S6K, SGK, RSK, and protein kinase C (PKC) isoforms. Upon cell stimulation, PDK1 is enabled to phosphorylate the T loops of all these AGC kinases, resulting in their activation (17, 18).

Since PDK1 is constitutively active in cells, the previous phosphorylation of a second activating residue located in a C-terminal conserved hydrophobic motif becomes rate limiting for PDK1 to bind and activate most substrates. The phosphorylated hydrophobic motif acts in this manner as a substrate-docking site recognized by a small groove within the PDK1 catalytic domain termed the PIF pocket (19, 20). In contrast, phosphorylation of Akt at the hydrophobic motif is not required for PDK1 to activate the kinase. The exclusive presence in both PDK1 and Akt of pleckstrin homology (PH) domains able to specifically interact with PtdIns(3,4,5)P₃ results in their colocalization at the plasma membrane, where PDK1 can phosphorylate and activate Akt (16).

The final demonstration that these two mechanisms operate *in vivo* came from analysis of two single-amino-acid, rationally designed PDK1 mutations abrogating the function of either the PH domain or the PIF pocket motif (21). We recently reported how in

Received 15 April 2016 Returned for modification 13 May 2016

Accepted 15 September 2016

Accepted manuscript posted online 19 September 2016

Citation Cordón-Barris L, Pascual-Guiral S, Yang S, Giménez-Llort L, Lope-Piedrafitra S, Niemeyer C, Claro E, Lizcano JM, Bayascas JR. 2016. Mutation of the 3-phosphoinositide-dependent protein kinase 1 (PDK1) substrate-docking site in the developing brain causes microcephaly with abnormal brain morphogenesis independently of Akt, leading to impaired cognition and disruptive behaviors. *Mol Cell Biol* 36:2967–2982. doi:10.1128/MCB.00230-16.

Address correspondence to Jose R. Bayascas, joseramon.bayascas@uab.cat.

* Present address: Lluís Cordón-Barris, GIGA-Neurosciences, Université de Liège, Liège, Belgium.

Copyright © 2016, American Society for Microbiology. All Rights Reserved.

PDK1^{K465E/K465E} knock-in mice, which express a mutant form of PDK1 incapable of phosphoinositide binding, activation of Akt was selectively affected. As a consequence, the ability of hippocampal and cortical embryonic neurons to differentiate was markedly impaired (22).

Full knock-in mice expressing a mutant form of PDK1 in which the leucine residue at position 155 within the PIF pocket was replaced by glutamic acid (L155E) were previously generated and died at midgestation. In the PDK1^{L155E/L155E} mice, activation of all the PDK1-regulated substrates with the exception of Akt was totally abolished (23). To define the contribution of PDK1 signaling beyond Akt to neurodevelopmental regulation, here we targeted the expression of the PDK1 L155E mutant protein to the developing brain. The PDK1 mutant mice were microcephalic, with neuronal polarization and axonal elongation significantly inhibited in the mutant neurons. As a consequence, the patterning of the brain was dramatically perturbed, as demonstrated by cortical layering alterations and reduced circuitry. This resulted in impaired cognition, along with abnormal behavior, which further highlights the importance of PDK1 targets different from Akt in mediating signaling responses that are key to brain development.

MATERIALS AND METHODS

Mice. The nestin-Cre transgenic mice were kindly provided by Ulrich Mueller at the Scripps Research Institute (24), whereas the PDK1 L155E conditional knock-in mice and the genotyping procedures were previously described (25). Animal maintenance conditions and experimental research were in accordance with publication 2010/63/UE regarding the care and use of animals for experimental procedures. The study complies with the ARRIVE guidelines developed by the NC3Rs (26).

Primary cultures. Neuronal primary cultures were established from embryonic day 15.5 (E15.5) embryos as previously described (22). Cortical cells were plated at a density of 20×10^4 cells/ml on plates coated with 50 μ g/ml of poly-D-lysine and maintained for 6 days *in vitro* (DIV) before treatments, whereas hippocampal cells were plated at a density of 7.5×10^4 cells/ml on 12-mm glass coverslips coated with 150 μ g/ml poly-D-lysine and placed in 24-well plates for 4 days *in vitro*.

MRI analysis. Adult mice were terminated, their brains were dissected, and the right hemispheres were kept at -80°C for biochemical analysis. The left hemispheres were fixed for 2 h in 4% paraformaldehyde, preserved in 70% ethanol solution at 4°C , and embedded in 1.5% agarose in phosphate-buffered saline (PBS). 1H magnetic resonance imaging (MRI) studies were performed in a 7T Bruker BioSpec 70/30 USR spectrometer equipped with a mini-imaging gradient set (400 mT/m), a 72-mm inner-diameter circular polarized linear transmitter volume coil, and a received-only mouse head surface coil. Images were acquired using a multislice fast low-angle shot (FLASH) sequence from the Bruker ParaVision 5.1 library (repetition time, 450 ms; echo time, 5.4 ms; excitation flip angle, 40°) in 33 contiguous 0.5-mm-thick slices, an acquisition matrix of 256 by 256, and a field of view of 19.2 mm by 19.2 mm, giving a voxel resolution of 0.0028125 mm^3 . The imaging data were Fourier transformed in ParaVision and then visualized using ImageJ software.

Determination of organ volume and cell size. Organ volume was determined using the Cavalieri method (27) applied to either MRI data sheets of the adult brain or physical sections of embryonic brain samples. MRI images were displayed in ImageJ and outlined, and the total number of pixels was multiplied by the voxel resolution and by a factor of 2 to obtain the adult brain volume, which was assumed to be twice the volume of one hemisphere. Embryonic brain paraffin-embedded sections 5 μ m thick were collected at systematically spaced locations (where the distance between sections $[k]$ was 96 μ m) from a random starting position and photographed with a Nikon SMZ800 stereomicroscope at $\times 1$ magnification using a digital camera. A square lattice grid of 0.9149 mm^2 (d^2) was

then overlaid on the photograph using the program Photoshop vCS5.1, and the number of intersections (P) hitting either the whole head or the brain was scored. The volume was estimated by using the formula $\Sigma P \times d^2 \times k$. The number and size of the cells were determined on E15.5 dissociated cortex tissues with a Scepter 2.0 handheld automated cell counter (Millipore).

Evaluation of neuronal proliferation, apoptosis, and survival. For the survival studies, cortical neurons obtained at E15.5 were cultured in complete neurobasal medium with the B27 supplement for 6 days *in vitro*, washed twice with Dulbecco's modified Eagle's medium (DMEM) without serum, and then either reincubated in conditioned medium or trophic factor deprived for 24 h in serum-free neurobasal medium in the absence or presence of 50 ng/ml of brain-derived neurotrophic factor (BDNF) (Alomone). Cell viability was determined by the MTT [3-(4,5-dimethylthiazol-2-yl)-2,5-diphenyltetrazolium bromide] reduction assay, whereas the percentage of apoptosis was determined after Hoechst staining by scoring the number of cells with fragmented or condensed nuclei, as described previously (22). For the proliferation and apoptosis studies, E15.5 cortical neurons were cultured in complete neurobasal medium supplemented with B27 for the indicated number of days *in vitro* and then processed for immunocytochemistry with antibodies recognizing the Ki67 proliferation marker and the active caspase 3 apoptotic marker.

Immunocytochemistry. Cells were fixed in 4% paraformaldehyde in PBS for 20 min at room temperature; rinsed twice with PBS; permeabilized with 0.02% saponin diluted in PBS for 7 min at room temperature; and blocked with 5% bovine serum albumin (BSA), 0.01% saponin, 10 mM glycine in PBS for 1 h at room temperature. Primary antibodies diluted in PBS with 0.01% saponin and 1% normal goat serum were incubated overnight at 4°C . The cells were then incubated with the appropriate secondary antibodies diluted 1:400 in the same solution for 90 min and counterstained with 1 μ g/ml of Hoechst 33342 (ThermoFisher no. H1399) for 30 min. Coverslips were mounted on microscope slides with FluorSave (Calbiochem no. 345789) reagent.

Evaluation of differentiation. Hippocampal cells fixed at different days *in vitro* were immunostained with the dendritic marker MAP2 and the axonal marker Tau-1 and counterstained with 1 μ g/ml of the nuclear dye Hoechst 33342. Images for the green, red, and blue channels were taken simultaneously with an epifluorescence microscope (Nikon Eclipse 90i) interfaced with a DXM 1200F camera at $\times 20$ magnification. The numbers and lengths of axons, dendrites, and dendritic branches and the soma diameter were measured with the NeuronJ plugin and scored with the cell counter from ImageJ 1.42q (Wayne Rasband, National Institutes of Health).

Generation of protein extracts and Western blot analysis. E15.5 cortical neurons cultured for 6 days *in vitro* in complete neurobasal medium supplemented with B27 were starved for 4 h in neurobasal medium without B27 and subsequently stimulated with 50 ng/ml BDNF for 15 min. Cells were scraped from the wells in ice-cold lysis buffer (50 mM Tris-HCl, pH 7.5, 1 mM EGTA, 1 mM EDTA, 1 mM sodium orthovanadate, 50 mM sodium fluoride, 5 mM sodium pyrophosphate, 10 mM sodium-glycero-phosphate, 0.27 M sucrose, 1%, [wt/vol] Triton X-100, 0.1% [vol/vol] 2-mercaptoethanol, and a 1:100 dilution of protease inhibitor cocktail; Sigma). Tissue extracts were prepared by homogenizing the frozen tissues on ice in a 10-fold volume excess of ice-cold lysis buffer using a Polytron (10674; Kinematika GmbH). The lysates were centrifuged at 4°C for 10 min at 13,000 rpm, and the supernatants were aliquoted and preserved at -20°C . Protein concentrations were determined by the Bradford method using bovine serum albumin as a standard. The activation states of the different pathways were assessed by immunoblotting the extracts (10 μ g) with the indicated antibodies, which were detected with the appropriate horseradish peroxidase-conjugated secondary antibodies. Membranes were incubated with the enhanced chemiluminescence (ECL) reagent and then either exposed to Super RX Fujifilm and developed, or detected using a ChemiDoc MP imaging system (Bio-Rad), and then quantified using ImageJ software.

Affinity purification of PDK1. Streptavidin-Sepharose (10 μ l; GE Healthcare) was conjugated to 0.5 μ g of biotinylated PIF peptide (biotin-C₆ spacer-REPRILSEEEQEMFRDFAYIADWC) and incubated with 0.3 mg of precleared tissue lysates at 4°C overnight on a shaking platform. The pulldown products were washed twice with 1 ml of lysis buffer supplemented with 150 mM NaCl, resuspended in sample loading buffer, electrophoresed, and then immunoblotted for PDK1.

Antibodies. The Akt and PRAS40 total antibodies were kindly provided by Dario Alessi, University of Dundee. The PDK1 (no. 3062), TrkB Tyr706/707-P (no. 4621), TrkB (no. 4603), Akt Thr308-P (no. 4056), Akt Ser473-P (no. 4060), PRAS40 Thr246-P (no. 2997), pan-PDK1 site PKC γ Thr514-P (no. 9379), S6K Thr389-P (no. 9234), S6K (no. 9202), S6 protein Ser235/236-P (no. 4858), S6 protein (no. 2217), ERK1/2 (no. 9102), RSK Ser380-P (no. 9335), and RSK 1/2/3 (no. 9355) antibodies were purchased from Cell Signaling Technology. The RSK Ser227-P (no. 12445) antibody was obtained from Santa Cruz Biotechnology, the SGK1 antibody (no. S5188) from Sigma, and the PKC α antibody (no. P16520) from Transduction Laboratories. Secondary antibodies were from Pierce.

For immunofluorescence experiments, we used the Tau-1 (no. MAB3420), GAD67 (no. MAB5406), parvalbumin (no. MAB1572), and NeuN (no. MAB377) antibodies from Millipore; the pan-axonal neurofilament (no. SMI-312R) antibody from Covance; the rabbit MAP2 (no. M3696) antibody from Sigma; the CUX1 (no. 13024) antibody from Santa Cruz Biotechnology; the Ki67 (no. ab156956) and doublecortin (no. ab18723) antibodies from Abcam; and the caspase 3 cleaved (no. 9661) antibody from Cell Signaling Technology. Alexa Fluor 594-conjugated goat anti-rabbit (no. A11072), Alexa Fluor 488-conjugated goat anti-mouse (no. A11017), and Alexa Fluor 594-conjugated goat anti-rat (no. A11007) secondary antibodies were obtained from Molecular Probes (Life Technologies).

Immunohistochemistry. Adult mice were intraperitoneally anesthetized with 0.4 mg/g body weight of pentobarbital, and then, an intracardiac injection of 70 heparin units was administered before perfusion with 0.9% NaCl, followed by 4% buffered paraformaldehyde. Brains were extracted, postfixed for 2 h in 4% paraformaldehyde, and preserved in 70% ethanol solution at 4°C. Embryos were dissected from E15.5 plug-tested pregnant females and decapitated, and the whole heads were fixed for 2 h in 4% paraformaldehyde and then preserved in 70% ethanol solution at 4°C. In both cases, samples from three littermates of different genotypes were embedded in the same paraffin block, with three as the final number of blocks, which were then sliced into 5- μ m-thick coronal sections with a Leica RM2255 microtome. The sections were dry heated for 2 h at 60°C; rehydrated; boiled for 10 min in 10 mM sodium citrate, pH 6, for antigen retrieval; cooled for 30 min on ice; and washed three times with Tris-buffered saline (25 mM Tris, pH 7.5, 150 mM NaCl) (TBS). Samples were blocked in TBS containing 0.02% Triton and 5% goat serum for 30 min and incubated overnight at 4°C with primary antibodies diluted in the same blocking solution. The sections were rinsed with TBS buffer, incubated for 1.5 h at room temperature with the corresponding secondary antibodies diluted 1:400 in TBS, and counterstained with 1 μ g/ml Hoechst 33342 before mounting in FluorSave reagent. Immunostained sections were photographed with a Nikon Eclipse 90i epifluorescence microscope, and the captured images were processed and analyzed with ImageJ 1.42q (Wayne Rasband, National Institutes of Health) and Fiji (http://pacific.mpi-cbg.de/wiki/index.php/Main_Page) software.

Behavioral analysis. A sample of 12-month-old female mice (six PDK1^{fl/fl} CRE⁺ mutants and six PDK1^{+/fl} CRE⁺ matched controls) were confronted with a standardized battery of behavioral tests (28, 29) administered over 10 consecutive days for preliminary screening of the behavioral phenotypes of the mutant mice. On day 1, observation of undisturbed behavior in the home cage, including sociability, barbering, and sleeping in a group pattern, was immediately followed by the assessment of several sensorimotor tasks. Motor coordination and equilibrium were assessed in the wooden and wire rod tests by the distance covered and the latency to falling off a horizontal 1.3-cm-wide wooden rod and a 1-cm-

diameter wire rod in two consecutive 20-s trials. Prehensibility and motor coordination were measured as the distance covered on the wire hang test, where the animals were allowed to cling with their forepaws for two trials of 5 s and a third, 60-s trial. Muscle strength was measured as the time needed to fall off the wire in the 60-s trial. Nesting behavior using paper towels was measured in isolation (housing conditions on day 10), according to Deacon's 5-point scale (30). The secondary and tertiary screens addressed neuropsychiatric-like deficits by assessing spontaneous exploratory behavior, anxiety-like behavior, circadian activity, and cognition in a series of tests involving different degrees of complexity. Neophobia in the corner test was recorded on day 2 in a new home cage by the horizontal (number of visited corners) and vertical (number and latency of rearings) activity during a period of 30 s. Immediately after, exploratory activity and anxiety-like behaviors in a standard open-field test were measured for 10 min. Horizontal (centimeters) and vertical (rearings) locomotor activities were recorded for each minute of the test. The following items of behavior were recorded: freezing (latency of initial movement), thigmotaxis (latency of leaving the central square and that of entering the peripheral ring 10 cm from the walls), and self-grooming behavior (latency, number, and duration of groomings). Defecation and urination were also measured. On day 3, a marble-burying test was performed in standard cages containing 10 glass marbles (1 by 1 by 1 cm) evenly spaced on a 5-cm-thick layer of sawdust. Latency to contacting a marble was measured, and at the end of the 30-min test, the number of marbles was determined as follows: intact (the number of unmanipulated marbles), change in position (the number of marbles at least half buried in sawdust and rotated 90° or 180°), and buried (the number of marbles 100% buried in sawdust) (30). On the next 3 days (days 4 to 6), perceptual visual learning and spatial learning and memory were assessed in a 3-day water maze. The animals were trained to a criterion (90% escaping in under 60 s) in a series of cued visible-platform trials (7-cm-diameter platform 1 cm above the water surface, with the position of the platform indicated by a visible 5- by 8-cm striped flag; 20-min intertrial time) in a pool (Intex Recreation Corp., CA; 91-cm diameter; 40 cm deep; 25°C opaque water). This required four platform trials (cued visible-platform trial 1 [CUE1] to CUE4). The last visible-platform trial of any animal was considered to be its posthabituation baseline and was designated CUE4. Mice that failed to find the platform within 60 s were manually guided to the platform and placed on it for 5 to 10 s, the same period as successful animals. Twenty-four hours after the last cued platform trial, the animals were tested in a series of four hidden-platform trials (PT1 to PT4, 20 min apart). In these place-learning tasks, the hidden platform (1.5 cm below the water surface) was located in a new position opposite the one used for cue learning. Escape latencies were measured with a stopwatch. Episodes of immobility (flotation) were measured. On days 7 to 10, circadian motor activity was tested for 84 consecutive hours in a home cage equipped with a running wheel (31).

Statistical analysis. Two-way analysis of variance and Student's *t* test analysis were applied to compare differences among categories, as depicted in the figures. Data analysis was done using Prism software (GraphPad Software, La Jolla, CA).

RESULTS

Generation of neuron-specific PDK1 L155E knock-in mice. We followed the minigene conditional knock-in approach to limit the expression of the PDK1 mutant protein to the neuronal lineage (25). In this method, a conditional allele was constructed in which the wild-type protein was expressed from the endogenous locus through the first two PDK1 exons, whereas expression of the remaining coding region occurred through a LoxP site-flanked minigene DNA cassette consisting of the wild-type PDK1 open reading frame from exons 3 to 14 followed by the natural transcriptional termination and polyadenylation signals. The construct was designed so that upon CRE recombinase-mediated excision of the floxed minigene, a mutated version of exon 4 coding

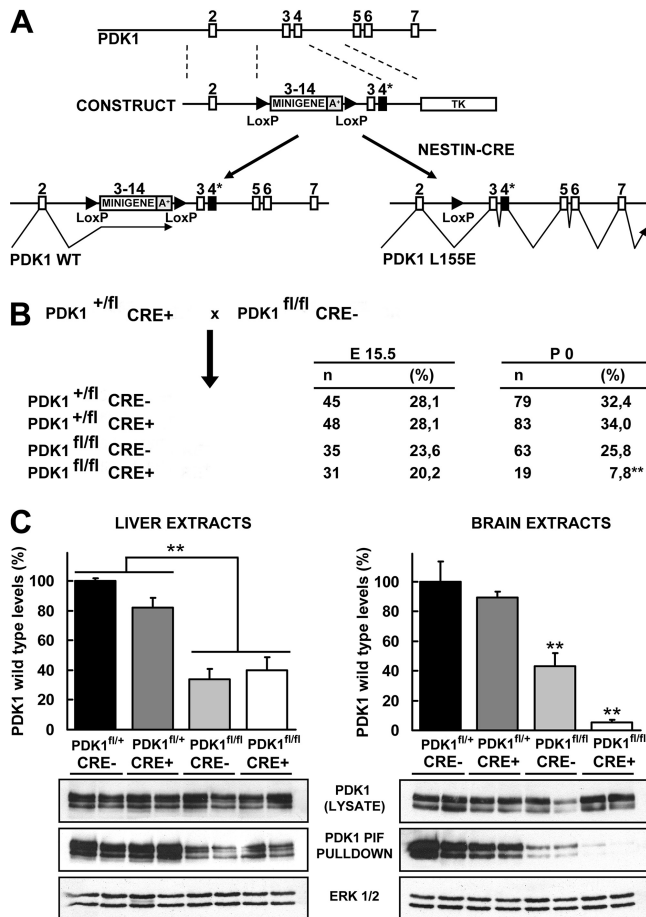


FIG 1 Generation of brain-specific PDK1 L155E mice. (A) Diagram depicting the 5' end of the PDK1 gene from exons 2 to 7 (PDK1); the targeting construct containing the thymidine kinase (TK) negative selectable marker and the minigene cassette, which includes the PDK1 open reading frame from exons 3 to 14 plus the natural polyadenylation signals (A^+) and is flanked by LoxP sites (CONSTRUCT); the targeted allele, which drives the expression of the PDK1 wild-type protein in control tissues (PDK1 WT); and the excised allele, in which the CRE recombinase-mediated deletion of the minigene cassette allows the expression of the PDK1 mutant protein (PDK1 L155E). The white boxes represent exons, the triangles represent LoxP sites, and the mutated exon 4 containing the Leu155Glu amino acid substitution is represented by black boxes labeled with asterisks. (B) Breeding strategy used for generation of mice expressing the PDK1 L155E mutant protein in brain. The number (n) and proportion (%) of mice of each genotype resulting from the depicted experimental breeding are indicated both at E15.5 and at birth (P0). **, the lower-than-expected frequency of $PDK1^{fl/fl} \text{ CRE}^+$ pups was statistically significant ($P < 0.005$ by χ^2 test). (C) PDK1 was affinity purified from liver or brain embryonic extracts of the indicated genotypes. The expression levels of the PDK1 wild-type protein were quantified on the indicated genotypes and tissues from the PDK1 immunoblot signals of the PIF-Sepharose pulldowns (middle blots), normalized by the total PDK1 protein levels derived from the whole tissue lysate immunoblot signals (upper blots), and represented as percentages of those of the $PDK1^{+/fl} \text{ CRE}^-$ controls (top). Each bar represents the means and standard errors of the mean for the immunoblot signals derived from two independent experiments. A representative Western blot is shown, where each lane corresponds to a sample derived from a different mouse. Immunoblots with the ERK1/2 antibody are also shown as controls for protein loading (bottom blots). **, $P < 0.005$ compared to controls.

for glutamic acid at position 155 of the mouse PDK1 protein would be transcribed (Fig. 1A).

A potential drawback of this floxed allele is its reported inability to efficiently use the termination signals of the minigene cas-

sette to finish transcription, which continued into the knock-in region of the gene even in the absence of CRE and produced significant amounts of mRNA for mutant PDK1 (25). However, we reasoned that this attribute, after the appropriate genetic crosses, would give rise to a valuable allelic series with increasing expression of the mutant PDK1 protein. Hence, mice homozygous for the PDK1 conditional transgene were crossed with nestin-CRE mice, which express the CRE recombinase under the control of the neuron-specific enhancer of the nestin promoter in precursors of both neurons and glia starting at E10.5 (24). The PDK1 L155E conditional floxed allele is referred to here as $PDK1^{fl/fl}$ for simplicity. $PDK1^{fl/fl} \text{ CRE}^+$ mice, but not $PDK1^{+/fl} \text{ CRE}^-$, $PDK1^{+/fl} \text{ CRE}^+$, or $PDK1^{fl/fl} \text{ CRE}^-$ mice, were born in a reduced Mendelian distribution (Fig. 1B). We confirmed that the PDK1 protein was expressed at similar levels in samples of the different genotypes analyzed (Fig. 1C). We next incubated protein extracts from either brain or liver with Sepharose conjugated to PIF-tide, a synthetic polypeptide corresponding to the amino acid sequence of the PDK1 substrate-docking site. PIF-tide interacts strongly with the PIF pocket of wild-type PDK1 but cannot interact with the PDK1 L155E mutant protein (32, 33). PDK1 could be affinity purified with high efficiency from $PDK1^{+/fl} \text{ CRE}^-$, $PDK1^{+/fl} \text{ CRE}^+$, and, to a lesser extent, $PDK1^{fl/fl} \text{ CRE}^-$ brain extracts but not from $PDK1^{fl/fl} \text{ CRE}^+$ mutant mouse brain extracts, thereby biochemically confirming the expected gradation in the expression of the mutant PDK1 L155E protein rather than the wild-type protein. As a control, we demonstrated that in liver tissues, which do not express CRE, PDK1 could be affinity purified with the same reduced efficiency from $PDK1^{fl/fl} \text{ CRE}^-$ and $PDK1^{fl/fl} \text{ CRE}^+$ mice, which are homozygous for the conditional leaky allele, in comparison to $PDK1^{+/fl} \text{ CRE}^-$ and $PDK1^{+/fl} \text{ CRE}^+$ controls, which retain a wild-type copy of the PDK1 gene (Fig. 1C).

The resultant $PDK1^{fl/fl} \text{ CRE}^+$ mutant mice, as well as the $PDK1^{fl/fl} \text{ CRE}^-$ mice, which also express high levels of the PDK1 L155E mutant protein in nonneuronal tissues (Fig. 1C), were viable and fertile and displayed a 25% reduction in body weight compared to $PDK1^{+/fl} \text{ CRE}^-$ mice, which retain a wild-type copy of the PDK1 gene (Fig. 2B).

Stereological analysis demonstrated that both the brain and head volumes were proportionally reduced by 20% in $PDK1^{fl/fl} \text{ CRE}^-$ and $PDK1^{fl/fl} \text{ CRE}^+$ E15.5 embryos compared to $PDK1^{+/fl} \text{ CRE}^-$ controls (Fig. 2A and C). While the $PDK1^{fl/fl} \text{ CRE}^-$ mice exhibited a 25% reduction in the volume and mass of the brain compared to the $PDK1^{+/fl} \text{ CRE}^-$ controls, which is proportional to the reduction in body weight, the $PDK1^{fl/fl} \text{ CRE}^+$ adult mutant mice exhibited microcephaly, with brains showing a reduction of about 50% in volume and mass compared to those from the $PDK1^{+/fl} \text{ CRE}^-$ controls (Fig. 2D). Determination of the volume of the neuronal soma and the number of neurons purified at E15.5 from the embryonic cortex suggested that the small brain size of the $PDK1^{fl/fl} \text{ CRE}^-$ and $PDK1^{fl/fl} \text{ CRE}^+$ mice might be mostly due to a reduction in the size of the cells rather than to a reduced number of cells (Fig. 2E and F).

S6K, RSK, SGK, and PKC are not activated in the $PDK1^{fl/fl} \text{ CRE}^+$ brain. To define the importance of the PDK1 substrate-docking site in the ability of PDK1 to activate its different cellular targets, primary cultures of cortical neurons derived from littermate $PDK1^{+/fl} \text{ CRE}^-$, $PDK1^{fl/fl} \text{ CRE}^-$, and $PDK1^{fl/fl} \text{ CRE}^+$ embryos were stimulated with BDNF for 15 min. As a control for stimulation, the activation of the BDNF receptor TrkB was mon-

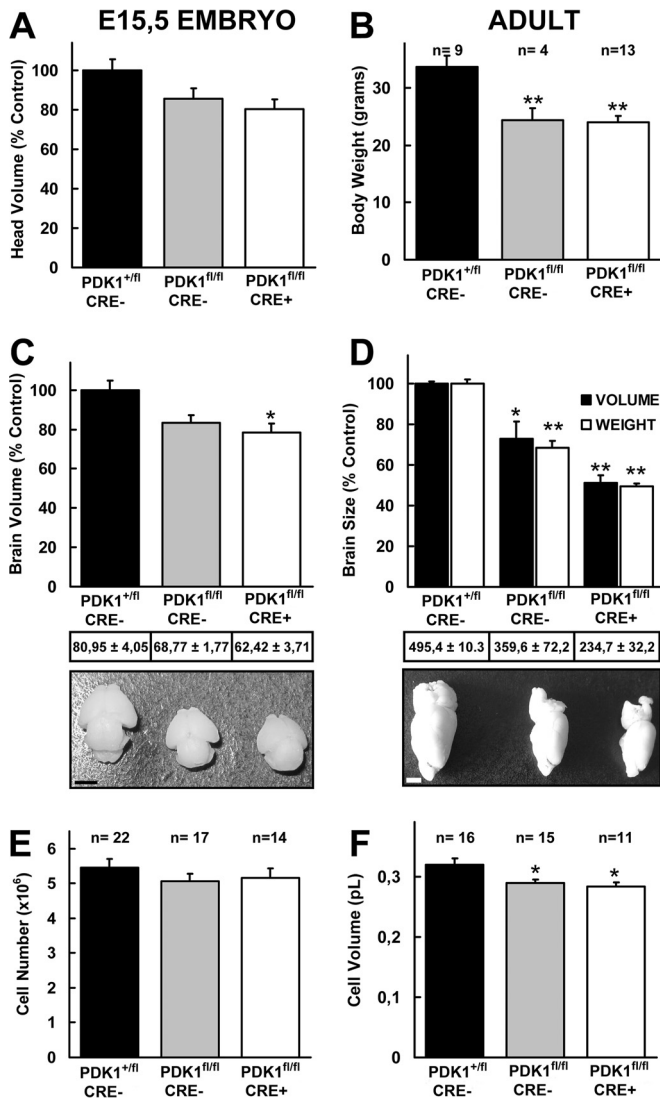


FIG 2 (A, C, and D) Microcephaly of PDK1^{fl/fl} CRE⁺ mice. The organ volume was measured from physical histological sections of the E15.5 embryo head (A) and brain (C) or MRI images of one hemisphere of the adult brain (D) by using the Cavalieri method, as described in Materials and Methods. The data are represented as means and standard errors of the mean obtained for three different mice per genotype and are expressed as percentages of the controls. (C and D) Total-volume values and representative photographs of E15.5 embryonic brains (C) or adult brain left hemispheres (D) are shown at the bottom, where the scale bars correspond to 1 mm and 2 mm, respectively. (B) Mean body weights of mice of the indicated genotypes. The values represent the means and standard errors of the mean for the indicated numbers of mice (n). (E and F) The number of cells (E) and the cellular volume (F) were determined from E15.5 dissociated cortical neurons with a Scepter 2.0 handheld automated cell counter (Millipore). The data are represented as the means and standard errors of the mean for the indicated numbers of embryos obtained from 11 independent litters. *, $P < 0.05$; **, $P < 0.005$ compared to controls.

itored by measuring its phosphorylation at the activation loop residues Tyr706/707, which was very robust in all three genotypes analyzed (Fig. 3A). In contrast, phosphorylation of TrkB was not detectable in whole brain tissue lysates at E15.5, despite the high levels of expression of the receptor (Fig. 3B).

BDNF induced clear activation of Akt to the same extent in all three genotypes analyzed, as judged by the level of phosphoryla-

tion of the two activating residues, Thr308 and Ser473. This was corroborated by measuring the phosphorylation levels of the Akt substrate PRAS40 at Thr246, which was not affected by the PDK1 L155E mutation (Fig. 3A). To further validate these data in a more physiological context, the levels of phosphorylation and activation of Akt were also measured in whole protein extracts derived from the E15.5 developing brain, which were similar in all three different genotypes analyzed (Fig. 3B).

In contrast, phosphorylation of S6K at the T loop Thr229 site by PDK1 was markedly reduced in the PDK1^{fl/fl} CRE⁻ cell and tissue samples compared with the PDK1^{+/fl} CRE⁻ controls and almost abolished in the PDK1^{fl/fl} CRE⁺ samples. As a consequence, S6K activation, as monitored by the phosphorylation of the S6 ribosomal protein at Ser235, was similarly affected (Fig. 3).

BDNF also induced robust autophosphorylation of the Ser380 hydrophobic-motif site of RSK and the consequent recognition and phosphorylation of the Ser227 T loop site by PDK1 (34) in the PDK1^{+/fl} CRE⁻ control cells. In contrast, phosphorylation of RSK at Ser227 by PDK1 was gradually reduced in the PDK1^{fl/fl} CRE⁻ and PDK1^{fl/fl} CRE⁺ cells and tissues (Fig. 3).

Activation of SGK1 requires the phosphorylation of the hydrophobic motif at Ser422 by mTORC2, which primes the binding of PDK1 (35). As expected, BDNF-induced phosphorylation of SGK1 at the Thr256 PDK1 site within the T loop was reduced in the PDK1^{fl/fl} CRE⁻ cortical cultures compared with the PDK1^{+/fl} CRE⁻ controls and further decreased in the PDK1^{fl/fl} CRE⁺ samples and tissues (Fig. 3).

PDK1 also controls the stability of PKC isoforms through the phosphorylation of their T loop sites (36). We found that both the levels of phosphorylation and the levels of expression of PKC α were reduced in the PDK1^{fl/fl} CRE⁺ cells and tissues (Fig. 3) compared to the PDK1^{fl/fl} CRE⁻ and PDK1^{+/fl} CRE⁻ samples.

Binding of the PDK1 PIF pocket to the substrate-docking site is not essential to support neuronal survival. The neuron-specific PDK1 PIF pocket mutation most likely compromised growth responses during brain development, leading to microcephaly in the PDK1^{fl/fl} CRE⁺ mutant adult mice. It is well known that the PI3K/PDK1/Akt signaling pathway plays critical roles in mediating the responses to survival signals that antagonize the intrinsic programmed cell death in the developing nervous system (6, 37). We recently showed how decreasing the efficiency of PKB/Akt activation by expressing the mutant form of PDK1 K465E, which is incapable of phosphoinositide binding, had no consequences for neuronal survival (22). From that, it was postulated that either the reduced levels of Akt activity attained in the PDK1^{K465E/K465E} mice were sufficient to preserve normal neuronal viability or that PDK1-activated kinases other than Akt were responsible for transducing the survival program elicited by extracellular signals. To address this question, we took advantage of the PDK1 L155E neuron-specific knock-in mice. Neuronal programmed cell death can be accurately recapitulated *in vitro* in primary cultures of embryonic cortical neurons, which survive in the presence of particular neurotrophins, such as BDNF, and die through apoptosis upon trophic factor withdrawal. Trophic factor deprivation induced the death of about half of the cells, as evidenced by a 50% decrease in the MTT reduction values (Fig. 4A) and a 5-fold increase in the number of apoptotic cells (Fig. 4B and C) in all four genotypes analyzed. BDNF completely restored the cell viability values (Fig. 4A) while decreasing by 2- to 3-fold the number of cells exhibiting apoptosis (Fig. 4B and C), to the same extent in all four genotypes

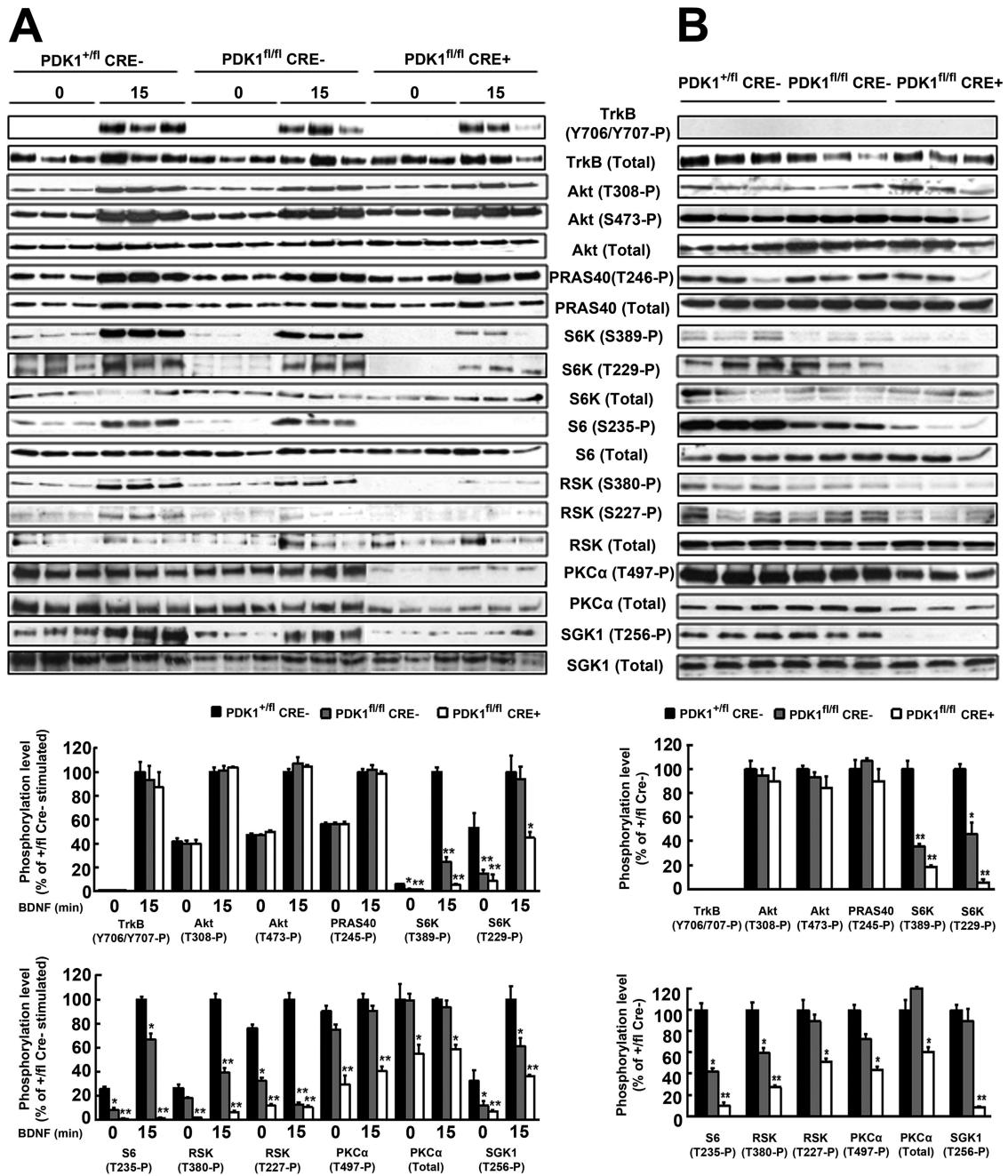


FIG 3 Activation of S6K1, RSK, SGK1 and PKC but not Akt is inhibited in PDK1^{fl/fl} CRE⁺ mice. (A) Cortical neurons from three independent embryos of the indicated genotypes were cultured for 6 DIV and then serum starved for 4 h and either left unstimulated (0) or stimulated with 50 ng/ml of BDNF for 15 min (15). (B) Whole-brain protein extracts were obtained at E15.5 from three independent embryos of each depicted genotype. Lysates were immunoblotted with the indicated antibodies to monitor the activation of Akt, S6K, RSK, SGK, and PKC. Each lane corresponds to a different embryo. Band densitometry quantification of the ratio between phosphorylated and total protein levels is shown at the bottom, where the bars represent the means and standard errors of the mean obtained for three different mice per genotype analyzed, and is expressed as a percentage of the BDNF-stimulated control samples (A) or control brain tissue samples (B). *, $P < 0.05$; **, $P < 0.005$ compared to controls.

analyzed. From this, it was concluded that the PDK1 PIF pocket-dependent AGC kinases were not essential for the neuroprotective actions of BDNF, at least in cortical neurons.

We next measured proliferation, as well as cell death parameters, in primary cultures of cortical neurons during the first 4 days *in vitro* by using the Ki67 proliferation marker and the cleaved/

active caspase 3 apoptotic marker. At DIV0, the PDK1^{+/fl} CRE⁻ control cultures reached their highest proliferation rates, above 20%, which were significantly reduced in both the PDK1^{fl/fl} CRE⁻ and PDK1^{fl/fl} CRE⁺ cultured cortical neurons (Fig. 5A and B). This proliferation activity, most likely corresponding to the neurogenesis peak of the progenitors that would later populate the

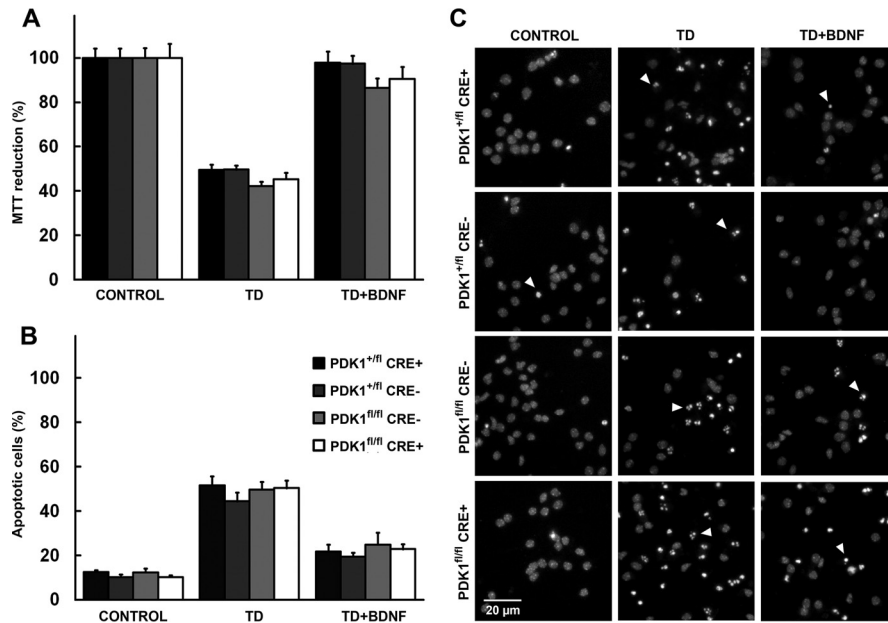


FIG 4 Neuronal survival responses are preserved in PDK1^{fl/fl} CRE⁺ mice. Cortical cells of the indicated genotypes were either sham treated (CONTROL) or deprived of trophic factors in the absence (TD) or presence of 50 ng/ml of BDNF (TD+BDNF) for 24 h. The data represent the means and standard errors of the mean for at least 3 independent mouse embryos per genotype from 6 independent litters. (A) Viability was determined with the MTT reduction assay and is expressed as a percentage of the untreated cells. (B) The percentage of apoptotic cells was obtained by scoring the numbers of nuclei exhibiting chromatin fragmentation from six different fields per well and 4 wells per condition divided by the total. (C) Representative micrographs of Hoechst-stained cortical neurons of the indicated genotypes after 24 h of the indicated treatment; the arrowheads indicate apoptotic nuclei.

upper cortical layers, mostly ceased as the cells progressed to DIV4, which was accompanied by a moderate increase in the apoptotic index to similar levels in all three genotypes analyzed (Fig. 5A and C). Accordingly, coronal brain sections from E15.5 embryos stained with the newborn neuron marker doublecortin revealed a clear reduction of the neuronal progenitor cells in PDK1^{fl/fl} CRE⁻ and PDK1^{fl/fl} CRE⁺ embryos compared to the PDK1^{+/+} CRE⁻ controls (Fig. 5D and E). In contrast, no evidence of apoptosis was observed in any of the three genotypes analyzed, as judged by the near absence of active caspase 3 staining (Fig. 5D and F). Since the soma size analysis of hippocampal neurons in culture revealed a genotype-dependent decrease in the diameter of the cellular soma (Fig. 6D), altogether, our data demonstrate a combined reduction in progenitor proliferation and cell growth responses.

PDK1 promotes neuronal polarization and axonal outgrowth through PIF pocket-dependent substrates. The PI3K signaling pathway controls several aspects of neuronal morphogenesis, including neuronal polarization, axonal outgrowth, and dendrite arborization (38). In PDK1^{K465E/K465E} mice, the Akt/mTORC1 axis regulated PI3K-mediated neuronal polarization and axon outgrowth (22). Since S6K is a major effector of mTORC1 in controlling the translation of proteins that are relevant for neuronal differentiation, we reasoned that the PDK1 L155E mouse model, with normal levels of Akt activity but in which S6K cannot be activated by PDK1, could be instrumental in defining the contribution of S6K to neuronal differentiation. To that end, we analyzed cell polarization and measured axon length during the differentiation of hippocampal primary neurons in culture. In the PDK1^{+/+} CRE⁻ control cultures, most of the neurons exhibited a differentiated axon by DIV3, as evidenced by the

expression of the axon-specific microtubule-associated protein Tau-1. In contrast, neuronal polarization was severely impaired in both the PDK1^{fl/fl} CRE⁻ and PDK1^{fl/fl} CRE⁺ mutant hippocampal cultures, in which only half of the neurons showed axons by DIV3 and -4 (Fig. 6A and B). The complexities of the neuritic processes, as inferred from the number of neurites per cell (Fig. 6C), as well as their lengths and the numbers of ramifications (Fig. 6E), were similar in PDK1^{+/+} CRE⁻, PDK1^{fl/fl} CRE⁻, and PDK1^{fl/fl} CRE⁺ mouse hippocampal neurons at all the time points analyzed. In contrast, the average length of the axon was reduced by 30% in the PDK1^{fl/fl} CRE⁻ neurons and as much as 40% in the PDK1^{fl/fl} CRE⁺ neurons compared to the PDK1^{+/+} CRE⁻ control cells at both DIV3 and -4 (Fig. 6E).

Reduced connectivity and abnormal cortical layering in the adult mutant mouse brain. We next explored how the deficient differentiation abilities of the PDK1^{fl/fl} CRE⁻ and PDK1^{fl/fl} CRE⁺ embryonic neurons detected *ex vivo* had physiological consequences in the adult brain. Immunostaining of brain sections with antibodies to microtubule-associated proteins that are selectively localized in either axons (SMI32) or dendrites (MAP2) revealed a clear decrease in the density of axonal fibers in various regions of the PDK1^{fl/fl} CRE⁻ and PDK1^{fl/fl} CRE⁺ cortex (Fig. 7A) and hippocampus (Fig. 7B), in a genotype dose-dependent manner.

The PI3K signaling pathway also controls the radial migration of newborn cortical neurons during cortex development, resulting in an ordered arrangement of neurons into six different cortical layers. It has been proposed that Akt, but not mTORC1, controls cortical development downstream of PI3K activation (39). Since the neuronal differentiation program is integrated with the program of neuronal migration, we aimed

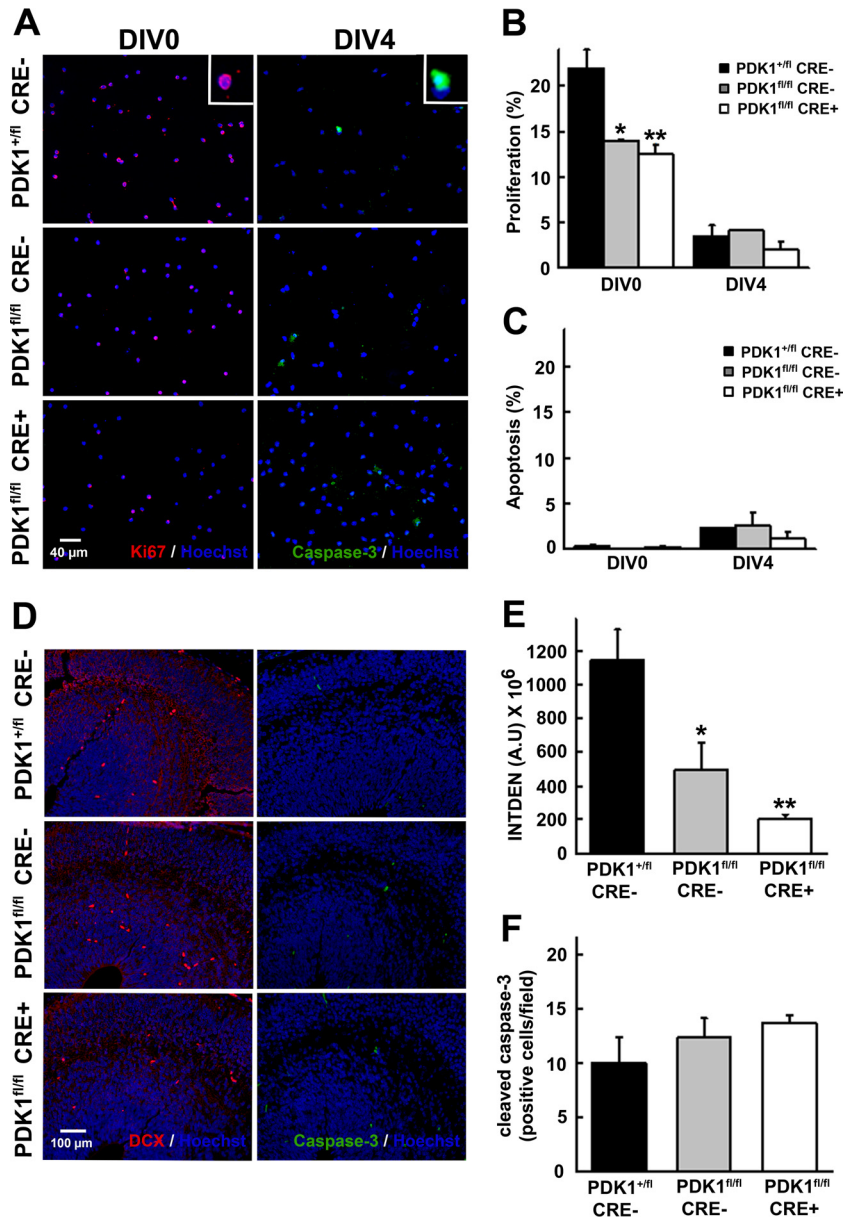


FIG 5 Reduced neuronal-progenitor proliferation in PDK1^{fl/fl} CRE⁻ and PDK1^{fl/fl} CRE⁺ embryos. (A) Representative micrographs of E15.5 embryonic cortical cultures of the indicated genotypes immunostained with the described antibodies. Insets show enlarged single-cell representative images of the nuclear staining of Ki67 in red and the cytoplasmic active caspase-3 staining in green. (B and C) The percentages of primary cortical neurons expressing the Ki67 proliferation marker (B) or the active caspase 3 apoptotic marker (C) were scored at the indicated time points. The bars correspond to the means and standard errors of the mean from 10 different fields per culture and three independent embryonic cultures per genotype. (D) Epifluorescence microscopy images of E15.5 embryonic brain coronal sections of the indicated genotypes immunostained with the described antibodies. DCX, doublecortin. (E and F) The intensity of doublecortin staining (INTDEN) (E) and the number of caspase 3-positive cells per field (F) were quantified and expressed as the means and standard errors of the mean from three independent sections per embryo obtained from three different embryos per genotype. A.U, arbitrary units. *, $P < 0.05$; **, $P < 0.005$ compared to controls.

to determine whether the PI3K/PDK1 effectors that are independent of Akt activation were also important for cortical development. We observed that in the PDK1^{fl/fl} CRE⁻ adult brain, neurons in layer IV of the somatosensory cortex were packed together (Fig. 8B) and further compacted in PDK1^{fl/fl} CRE⁺ mice (Fig. 8C) compared to the PDK1^{+/fl} CRE⁻ controls (Fig. 8A), as revealed by immunohistochemical analysis with the NeuN neuronal marker.

Cortical layer IV is mainly composed of pyramidal neurons

and GABAergic interneurons. For that reason, we employed antibodies against CUX1, a transcription factor that is expressed in glutamatergic cortical neurons from upper layers II to IV of the somatosensory cortex, and GAD67, the decarboxylase that catalyzes the conversion of glutamate to the GABA-inhibitory neurotransmitter in the GABAergic interneurons. While CUX1 staining confirmed that the neuronal packing arises from an increase in the glutamatergic-neuron density with an unchanged number of cells (Fig. 9A to D), a clear decrease in GAD67 expression in the

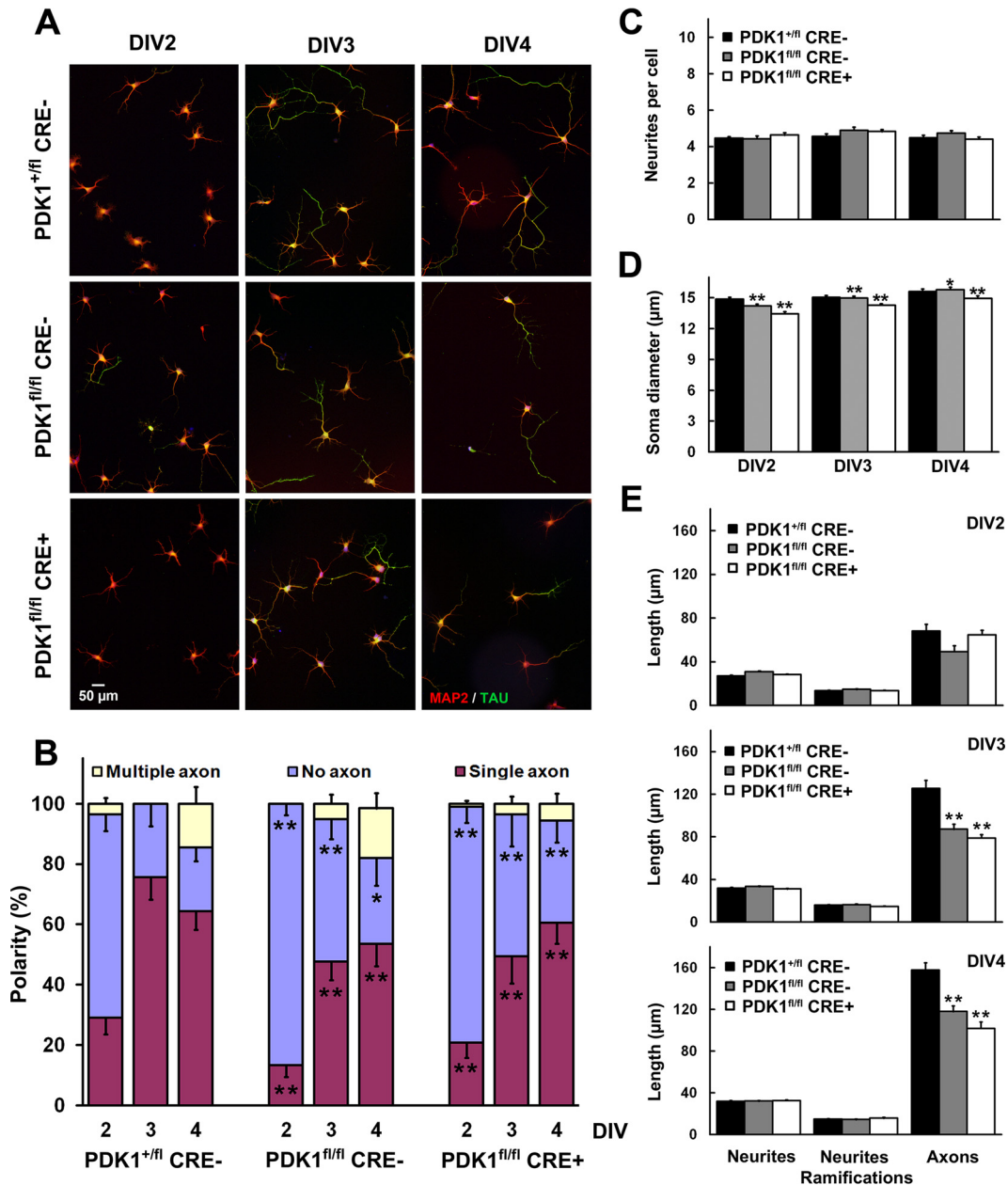


FIG 6 Deficient polarization and axonal outgrowth in PDK1^{fl/fl} CRE⁻ and PDK1^{fl/fl} CRE⁺ mice. (A) Representative micrographs of hippocampal cultures from the indicated genotypes at different DIV stained with the dendrite-specific marker MAP2 (red) and the specific axonal marker Tau-1 (green). (B to E) The percentage of polarization (B), the number of neurites per cell (C), the diameter of the soma (D), and the lengths of neurites, neurite ramifications, and axons (E) were measured at different time points on samples from the indicated genotypes. Each bar represents the means \pm standard errors of the mean for 100 neurons from three different embryos per condition. *, $P < 0.05$; **, $P < 0.005$ compared to controls.

somatosensory cortex (Fig. 9A and E) and the cingulate cortex (Fig. 9F) was observed, arising from the increase in the PDK1 L155E mutant protein levels across the different genotypes analyzed. Moreover, the parvalbumin-positive interneurons were mostly excluded from layer IV in the PDK1^{fl/fl} CRE⁺ cortex samples compared with its distribution in the PDK1^{fl/fl} CRE⁻ and PDK1^{+/fl} CRE⁻ cortices (Fig. 9B).

Neuropsychiatric-like behaviors in brain-specific PDK1 L155E mutant mice. A three-stage protocol for behavioral and functional comprehensive phenotype assessment of mutant mice

(28, 29) evaluated the physical condition, sensorimotor functions, behavioral and psychological profiles (spontaneous behavior, locomotor and exploratory activities, anxiety-like behaviors, and motivation), and cognition (learning and memory, attention, and executive functions). Somatic growth, as measured by body weight, was reduced, with lower food intake (Fig. 10A). Sensorimotor functions were severely (2-fold) reduced, even in an easy task, such as the wooden rod test (Fig. 10B). A deficiency in a highly preserved daily life ethological activity, such as nesting behavior, evidenced impairment of executive functions (Fig. 10C).

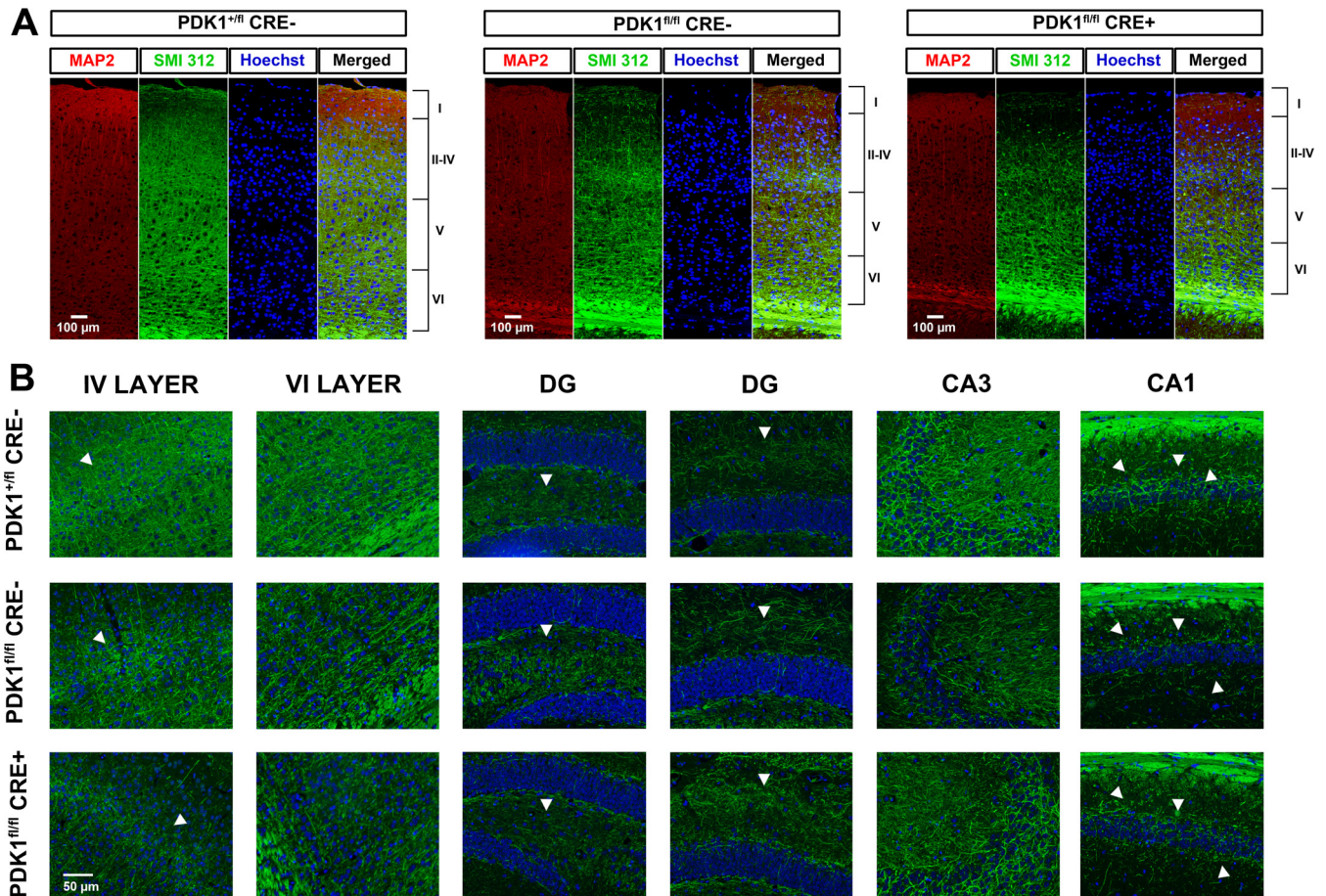


FIG 7 Reduced connectivity in $PDK1^{fl/fl} CRE^{-}$ and $PDK1^{fl/fl} CRE^{+}$ mouse brains. (A) Epifluorescence micrographs of coronal sections of the somatosensory cortex from mouse brains of the indicated genotypes stained with the dendrite-specific marker MAP2, the general axonal marker SMI312, and the nuclear Hoechst dye. Merged signals are also shown. The cortical layers are indicated on the right from I to VI. (B) Image magnifications of cortical layers IV and VI, as well as the hippocampal dentate gyrus (DG) and CA3 and CA1 regions stained with SMI312 and Hoechst dye. The arrowheads indicate differences in the densities of axonal fibers between genotypes.

The mutant mice showed apparently undisturbed behavior in the home cage, with normal socialization and sleeping in groups but absence of barbering. Disrupted behavior was aroused by handling, with a high incidence of hyperreactivity shown as refusal to be handled (5/6), vocalizations (3/6), bizarre behavior (4/6) (Fig. 10D) (stereotyped stretching), refusal to perform tests like the hanger test (6/6), and diminished motivation to swim in the water maze (Fig. 10G) (flotation). Neophobia in the corner test suggested flight behavior, which in a more anxiogenic environment, such as the open-field test (Fig. 10E), turned into freezing behavior. Overall reduced total vertical exploratory activity was observed, while the thigmotaxis ratio (locomotion in the periphery versus the center) was maintained in the mutants. These results were confirmed in the 84-h continuous circadian activity recordings in a cage equipped with a wheel (Fig. 10H). In that setting, the time course from the first (novelty) to the fourth (habituation) night was strikingly reduced in the mutant mice, mostly within the first two nocturnal activity periods. In the marble-burying test, the mutants exhibited a higher number of marbles changed in position, to the detriment of the number of buried pieces (Fig. 10F). With respect to their cognitive abilities, the two groups solved the first experience in the water maze equally well.

However, a poorer acquisition curve was seen in the mutant group, resulting in a worse cognitive capacity at the end of the perceptual visual learning paradigm, which involves attention and motivation (Fig. 10G, CUE1 to -4). Similarly, on the subsequent days, the mutant mice showed cognitive deficits in their spatial-learning and memory abilities in the place-learning task. They performed similarly in the first trial of each day (long-term memory) but did not progress successfully in the trial-by-trial test (short-term and working memory), again with worse learning curves and ratios than the age-matched wild-type group. A higher incidence of periods of immobility (flotation), as a nonsearching behavior indicative of changes in motivation in the mutants, was also shown throughout the test (Fig. 10G).

DISCUSSION

In the present study, we characterized the Akt-independent roles that the PDK1 signaling pathway plays during brain development. Disrupting the interaction of PDK1 with its substrates in the $PDK1^{L155E/L155E}$ full knock-in mice resulted in an embryonic-lethal phenotype, with embryos dying at E12 and exhibiting severe retardation and a major reduction in forebrain size, highlighting the essential roles that the Akt-independent branch of the PDK1

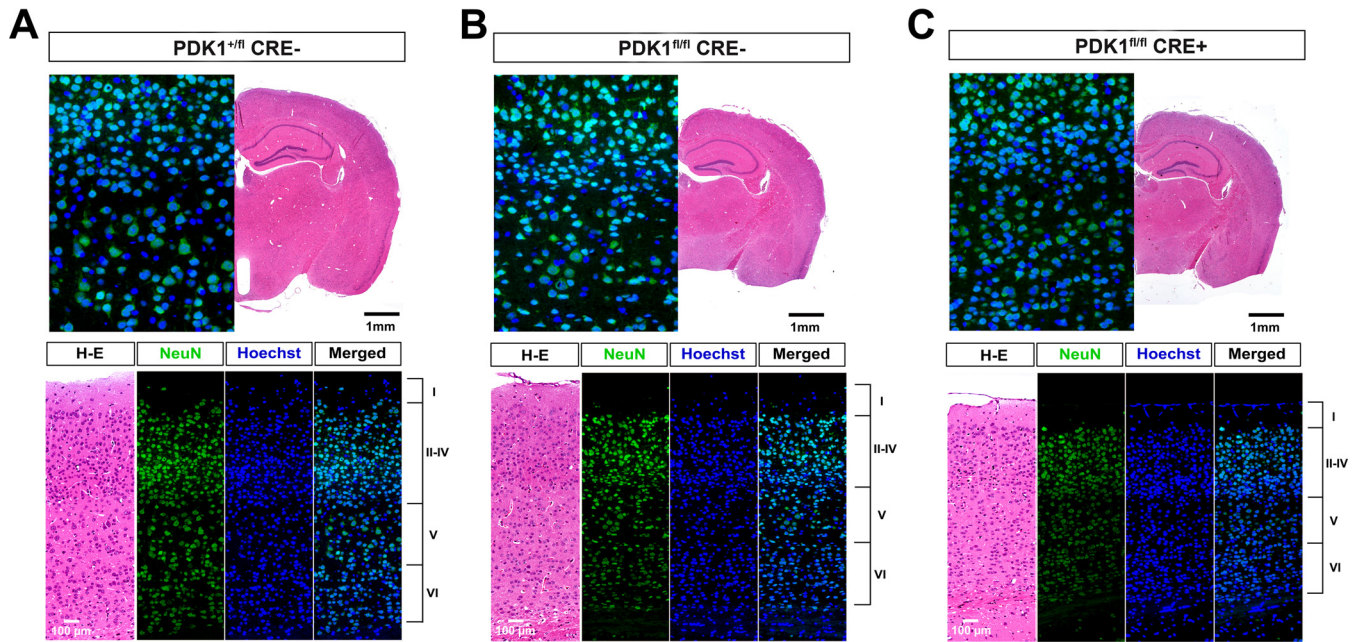


FIG 8 Abnormal cortical layering with compaction of layer IV in $PDK1^{fl/fl} CRE^{-}$ (B) and $PDK1^{fl/fl} CRE^{+}$ (C) mouse brains compared to the $PDK1^{+/fl} CRE^{-}$ controls (A). (Bottom) Epifluorescence microscopy images of coronal sections of the somatosensory cortex from mice of the indicated genotypes stained with the neuronal marker NeuN and the nuclear Hoechst dye, as indicated. Adjacent hematoxylin and eosin (H-E)-stained sections and merged signals are also shown. The cortical layers are indicated on the right from I to VI. (Top) Low-magnification micrographs of the H-E-stained sections and high-magnification images of the merged epifluorescence images corresponding to layers II to V.

signaling network plays during embryonic development (23, 40). To circumvent this lethal period, we targeted the expression of the PDK1 L155E mutant protein to neuronal tissues by conditional knock-in methodologies. The $PDK1^{fl/fl} CRE^{+}$ genotype was observed at birth at a 3-fold-reduced Mendelian frequency. In contrast, the $PDK1^{fl/fl} CRE^{-}$ mice were born at the expected frequency, indicating that low levels of PDK1 wild-type protein were sufficient for the $PDK1^{fl/fl} CRE^{-}$ mice to complete embryonic development and that the further and specific ablation of the wild-type PDK1 sequence in the nervous system was responsible for the lethality in the $PDK1^{fl/fl} CRE^{+}$ mutant embryos. The hypomorphic nature of the PDK1 L155E conditional knock-in allele, which can drive the expression of as much as 60 to 70% of PDK1 L155E mutant protein without compromising the viability of these mice, makes the $PDK1^{fl/fl}$ conditional knock-in mice an excellent genetic tool to study the function of PDK1, beyond Akt, in a more physiological context. At the same time, these mice could represent an appropriate experimental model to validate the effects of new allosteric modulators targeting the PDK1 PIF pocket that are now being developed and that have enormous therapeutic potential (41).

Activation of S6K, RSK, SGK, and PKC but not Akt was selectively decreased in the $PDK1^{fl/fl} CRE^{-}$ mouse cortical neurons compared to the $PDK1^{+/fl} CRE^{-}$ controls and further abolished in the $PDK1^{fl/fl} CRE^{+}$ neurons and tissues. We and others recently described how, in the absence of $PtdIns(3,4,5)P_3$ binding, PDK1 can still activate Akt by binding to the phosphorylated-Akt hydrophobic motif (42, 43). In agreement with that, in the $PDK1^{K465E/K465E}$ knock-in mice expressing a mutant form of PDK1 incapable of phosphoinositide binding, activation of Akt was selectively affected but not fully abolished (22). In contrast, in

the $PDK1^{fl/fl} CRE^{+}$ neurons and tissues, Akt was normally activated, demonstrating that under physiological conditions, Akt activation by PDK1 relies mostly on the phosphoinositide-mediated colocalization of both kinases at $PtdIns(3,4,5)P_3$ -rich cellular membranes rather than on the docking-site interaction.

The reduced phosphorylation of S6K and RSK at their activation loops by PDK1 arises from the inability of the PDK1 L155E mutated PIF pocket to interact with the phospho-hydrophobic-motif docking site in S6K and RSK. Unexpectedly, the level of phosphorylation of S6K at the Thr389 and of RSK at the Ser380 hydrophobic-motif sites was also decreased to the same extent as that of the activation loops. The AGC kinases possess a hydrophobic groove in the small lobe of their kinase domains similar to the PDK1 PIF pocket. This hydrophobic pocket establishes intramolecular interactions with the phosphorylated hydrophobic motif that are fundamental for the transition of the enzyme to the active conformation (44). In the absence of activation loop phosphorylation, the active, closed conformation is not favored, which may allow the exposure of the hydrophobic motif phosphorylation site to the action of phosphatases (23).

PDK1 plays a major role in the processing and maturation of several PKC isoforms. Newly synthesized PKC polypeptides are first phosphorylated at their hydrophobic motifs, allowing PDK1 to interact with and phosphorylate the T loops. These first phosphorylation events do not depend on apical agonist stimulation and stabilize the enzyme in a conformation that is catalytically inactive but at the same time competent to respond to the diacylglycerol and calcium second messengers (45, 46). In agreement with that notion, both the levels of phosphorylation and the levels of expression of PKC α were reduced in the $PDK1^{fl/fl} CRE^{+}$ embryonic-brain samples, as well as cortical cell extracts, but not in

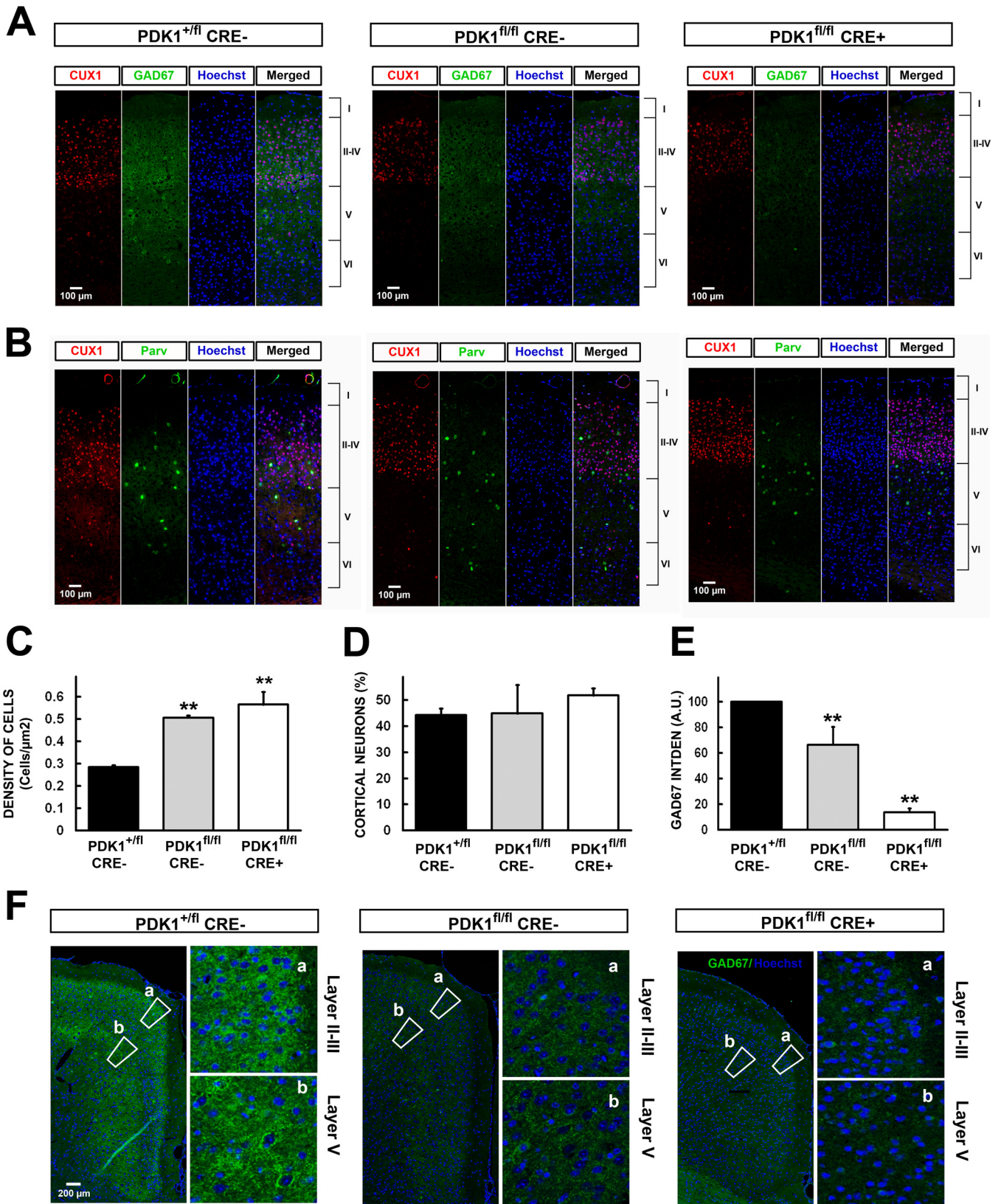


FIG 9 Reduced GAD67 levels and abnormal parvalbumin staining patterns in PDK1^{fl/fl} CRE⁻ and PDK1^{fl/fl} CRE⁺ mouse brains. (A and B) Epifluorescence microscopy images of coronal sections of the somatosensory cortex from mice of the indicated genotypes stained with the layer II- to IV-specific marker CUX1, the GABAergic neuron-specific marker GAD67, the interneuron marker parvalbumin, and the nuclear Hoechst dye, as indicated. The cortical layers are indicated on the right from I to VI. (C to E) The density of neurons in layer IV (C), the percentage of CUX1-positive neurons in layer IV among the total number of CUX1-positive neurons in layers I to IV (D), and the intensity of GAD67 staining (E) were quantified and expressed as the means and standard errors of the mean from three independent sections per embryo obtained from three different embryos per genotype. (F) Epifluorescence microscopy images of coronal sections of the cingulate cortex from mice of the indicated genotypes stained with the GABAergic neuron-specific marker GAD67 and the nuclear Hoechst dye. Higher-magnification images of layer II and III (a) and layer V (b) regions are also shown. **, $P < 0.005$ compared to controls.

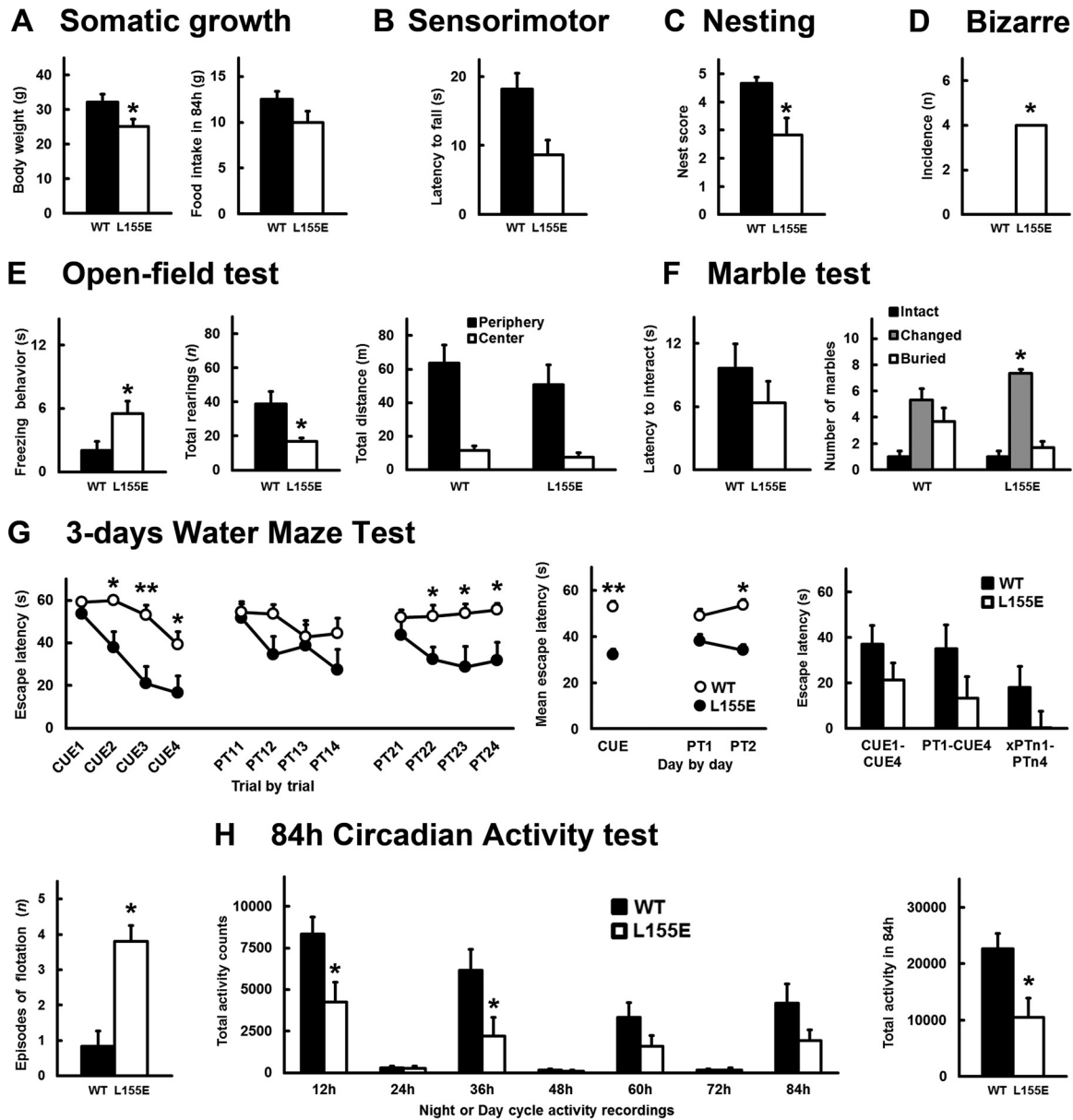


FIG 10 Disruptive behavior with diminished motivation and cognitive deficits in PDK1^{fl/fl} CRE⁺ mice. The somatic growth-related parameters (A), sensorimotor performance on the wooden rod test (B), executive functions in the nesting behavior daily life activity (C), incidence of bizarre behaviors (D), exploratory activity and anxiety-like behaviors in a standard open-field test (E), level of interaction in the marble-burying test (F), cognitive abilities in the water maze and depression-like diminished motivation measured by episodes of immobility (G), and circadian activity on running wheels (H) were assessed in six PDK1^{+/fl} CRE⁻ (WT) and six PDK1^{fl/fl} CRE⁺ (L155E) adult female mice. *, $P < 0.05$; **, $P < 0.005$ compared to controls. The error bars indicate the means and standard errors of the means.

the PDK1^{fl/fl} CRE⁻ samples compared to the PDK1^{+/fl} CRE⁻ controls (Fig. 3), indicating that the reduced levels of expression of the wild-type PDK1 protein in PDK1^{fl/fl} CRE⁻ mice were sufficient to regulate phosphorylation and stability of PKC isoforms, which was unchanged upon BDNF stimulation of cortical neurons (Fig. 3A).

One salient finding of these studies is that disrupting the interaction of PDK1 with its substrates in the PDK1^{fl/fl} CRE⁺ mutant mice had no consequences for neuronal survival. This is consistent with the fact that the PKB/Akt kinase, which is the only PDK1 substrate that is not affected by the PDK1 L155E mutation, is

thought to be the critical downstream effector of this pathway in promoting survival by antagonizing programmed cell death (47). However, in PDK1^{K465E/K465E} knock-in mice, reduced activation of Akt isoforms was also sufficient to dictate neuronal survival (22). We recently demonstrated how the inhibition of mTORC2, the Akt and SGK hydrophobic-motif kinase, modestly compromised the viability of PDK1 wild-type neurons at doses that did not affect Akt activation, and this was further aggravated in the PDK1^{K465E/K465E} mutant neurons (43). Altogether, these results point to a synergistic role for both Akt and SGK in controlling neuronal survival by coordinately regulating the phosphorylation

of some substrates that are relevant to the control of apoptosis. In contrast, both cell proliferation and cell growth were reduced in the PDK1^{fl/fl} CRE⁺ mutant mice, which might be due to the inability of PDK1 to activate S6K despite unaffected PI3K/Akt/mTORC1 signaling. These results implicate S6K as the most critical downstream effector of this signaling pathway in instructing cell and organism growth.

The observation that both the neuronal polarization and axonal elongation responses of hippocampal neurons from PDK1^{fl/fl} CRE⁻ and PDK1^{fl/fl} CRE⁺ mice were inhibited by the PDK1 PIF pocket mutation is particularly relevant, since the establishment of the axon-dendrite axis is an essential morphogenetic mechanism for the appropriate assembly of neurons into functional neuronal circuits. This process is triggered by different extracellular signals acting through a number of intracellular signaling pathways. Among them, the interplay between the PI3K/Akt signaling pathway (48), the Par3-Par6-atypical PKC complex (4), and the LKB1/BRSK axis (49, 50) is fundamental in controlling axon specification and growth. In agreement with this, in PDK1^{K465E/K465E} mice, the PI3K/Akt/mTORC1-dependent regulation of the BRSK protein levels represents an integration point for both the PI3K and LKB1 signaling pathways in axonal morphogenesis (22). In these mice, the hypomorphic reduction of Akt signaling toward the PRAS40/TSC2/mTORC1/S6K axis caused mild phenotypes that could be mimicked *ex vivo* with the Akti-1/2 inhibitor, which reduced Akt activity by inhibiting Akt1 and Akt2 but not the Akt3 isoform, and aggravated by using the mTORC1 inhibitor rapamycin. Interestingly, in PDK1^{fl/fl} CRE⁻ and PDK1^{fl/fl} CRE⁺ mice, in which the PI3K/Akt/mTORC1 axis is normally activated, the defects in both the polarity and axonal-elongation processes were more severe than those reported in PDK1^{K465E/K465E} mice, which phenocopied the severe differentiation defects previously observed with the mTORC1 inhibitor (22). Altogether, these observations place a PIF pocket-dependent kinase, namely, S6K, as a key effector of the PI3K/Akt/mTORC1 axis in controlling the synthesis of proteins that are relevant for neuronal morphogenesis. Moreover, while in PDK1^{K465E/K465E} mice the transient alterations in the timing of the differentiation program did not translate into gross abnormalities in the patterning of the adult brain (22), the genetic ablation of S6K activation with intact Akt signaling in PDK1^{fl/fl} CRE⁺ adult mice caused microcephaly with profound structural and molecular brain alterations, ruling out the implication of Akt or mTORC1 substrates other than S6K in these phenotypes.

Further experiments must be undertaken in the future to elucidate the connection between the impaired PDK1 PIF pocket-dependent signaling in mutant mice and the altered population of interneurons evidenced by the GAD67 and parvalbumin marker defects. In this regard, defects in the translation machinery in neurons caused by elongator subunit Elp3 deletion have been recently related to impaired neuronal differentiation and unbalanced neurogenesis, leading to microcephaly resulting from the premature differentiation of neurons (51, 52). In an analog form, the S6K PIF pocket-dependent kinase is indispensable for preinitiation complex (PIC) formation and protein translation (53, 54). Abrogation of S6K activation in PDK1 L155E mutant mice could have impaired the normal protein translation in neurons, leading to unbalanced neurogenesis, thereby generating a potential molecular connection between the PIF pocket mutation and the described brain defects associated with microcephaly. Moreover, the defi-

cient polarization and axonal outgrowth of the PDK1 L155E mutant neurons might have caused altered migration patterns during cortex lamination, contributing to the decreased density of axonal fibers in the cortex and hippocampus, increased density of glutamatergic neurons with normal numbers of cells in cortical layers II to IV, decreased GAD67 expression levels, and mislocalized parvalbumin-positive interneurons, which were mostly excluded from layer IV. Intriguingly, these alterations are commonly observed in human mental diseases, such as schizophrenia. They included reduced axonal density in the cortex and the hippocampus (55); elevated neuronal density in cortical layer IV (56); GAD67 deficits in the upper cortical layers, especially in the cingulate cortex (57); and abnormal localization of the parvalbumin-positive interneurons (58). The current hypotheses for the etiology of schizophrenia state that this molecular and structural scenario is thought to result in deregulated GABAergic interneuron-mediated inhibition of glutamatergic neurons, resulting in overactivation of the neuronal circuits and thus contributing to the characteristic symptoms of the disease.

In PDK1^{fl/fl} CRE⁺ mice, the behavioral disturbances included a wide array of impairments, ranging from sensorimotor and basic species executive functions to both cognitive and noncognitive behavioral alterations. The different tests assessed point to relevant and persistent bizarre behavior, severe reduction of exploratory activity, increased freezing, diminished motivation, and impaired short-term working memory. Much future work needs to be performed to determine whether the presence of exacerbated disruptive behavior, suggesting hypersensitivity to stressful situations, but reduced activity and diminished motivation have validity as negative symptoms that characterize the clinical features of the schizophrenia spectrum (59). Moreover, cognitive impairment affecting learning and memory, but also attention and executive functions, would also be compatible with cognitive clinical symptoms of schizophrenia.

Human schizophrenia might arise from an inherited genetic predisposition causing brain developmental alterations combined with environmental factors that can influence brain maturation during childhood. A number of genes that have been associated with familiar forms of schizophrenia converge on the same signaling pathway. They include the neuregulin 1 (NRG1) growth factor gene (60, 61), the dystrobrevin-binding protein 1 (DTNBP1) gene (12), the DISC1 scaffolding protein gene (13), and the Akt1 gene (11), which together participate in modulation of Akt signaling outputs. To our knowledge, this is the first report showing the involvement of PDK1 downstream effectors other than Akt in mouse neuropsychiatric-like disorders, with potential face and construct validity for negative and cognitive symptoms of schizophrenia. Our results point to a prominent function for PIF pocket-dependent kinases as major effectors of this signaling hub downstream of Akt in the etiopathogenesis of schizophrenia that might provide construct validity to the PDK1 L155E mutants.

ACKNOWLEDGMENTS

We thank Dario Alessi (MRC Protein Phosphorylation Unit, Dundee, United Kingdom) for providing the mice and some of the antibodies; Cristina Gutierrez, Mar Castillo, and Núria Barba (Cell Culture, Histology and Microscopy Services of the Institut de Neurociències) for technical assistance; Jessica Pairada and Núria Moix (Estabulari de Rosegadors of the Universitat de Lleida) for animal care; and the joint nuclear magnetic resonance facility of the Universitat Autònoma de Barcelona and

Centro de Investigación Biomédica en Red-Bioingeniería, Biomateriales y Nanomedicina (CIBER-BBN) (Cerdanyola del Vallès, Spain) for time allocated. We express our gratitude to Alfredo Miñano and Montse Solé for helpful discussion and to Arnaldo Parra, Lilian Enríquez, and Carles Saura for their expert advice on mouse brain development.

L.C.-B., J.R.B., J.M.L., and E.C. designed the experiments, analyzed the data, and wrote the manuscript. L.C.-B. performed most of the biochemical, cell biology, survival, differentiation, and brain anatomopathological experiments. S.P.-G. conducted the stereological analysis, as well as the proliferation and apoptosis studies. S.Y. and S.P.-G. carried out the signaling analysis. C.N. helped with the differentiation studies. S.L.-P. assisted with the MRI analysis. L.G.-L. carried out the behavioral characterization. J.R.B. managed and genotyped the mouse colonies.

We have no relevant conflicts of interest to disclose.

FUNDING INFORMATION

This work was funded by Ministerio de Economía y Competitividad (MINECO), Programa Estatal de Investigación, Desarrollo e Innovación Orientada a los Retos de la Sociedad (SAF2014-52813-R to J.R.B.). J.R.B. is a Serra Hünter Fellow of the Catalan Government. S.Y. was supported by a Fellowship of the China Scholarship Council. The funders had no role in study design, data collection and interpretation, or the decision to submit the work for publication.

REFERENCES

- Vanhaesebroeck B, Stephens L, Hawkins P. 2012. PI3K signalling: the path to discovery and understanding. *Nat Rev Mol Cell Biol* 13:195–203. <http://dx.doi.org/10.1038/nrm3290>.
- Engelman JA, Luo J, Cantley LC. 2006. The evolution of phosphatidylinositol 3-kinases as regulators of growth and metabolism. *Nat Rev Genet* 7:606–619. <http://dx.doi.org/10.1038/nrg1879>.
- Choi YJ, Di NA, Kramvis I, Meikle L, Kwiatkowski DJ, Sahin M, He X. 2008. Tuberous sclerosis complex proteins control axon formation. *Genes Dev* 22:2485–2495. <http://dx.doi.org/10.1101/gad.1685008>.
- Shi SH, Jan LY, Jan YN. 2003. Hippocampal neuronal polarity specified by spatially localized mPar3/mPar6 and PI 3-kinase activity. *Cell* 112:63–75. [http://dx.doi.org/10.1016/S0092-8674\(02\)01249-7](http://dx.doi.org/10.1016/S0092-8674(02)01249-7).
- Jiang H, Guo W, Liang X, Rao Y. 2005. Both the establishment and the maintenance of neuronal polarity require active mechanisms: critical roles of GSK-3 β and its upstream regulators. *Cell* 120:123–135. <http://dx.doi.org/10.1016/j.cell.2004.12.033>.
- Brunet A, Datta SR, Greenberg ME. 2001. Transcription-dependent and -independent control of neuronal survival by the PI3K-Akt signaling pathway. *Curr Opin Neurobiol* 11:297–305. [http://dx.doi.org/10.1016/S0959-4388\(00\)00211-7](http://dx.doi.org/10.1016/S0959-4388(00)00211-7).
- Chalhoub N, Zhu G, Zhu X, Baker SJ. 2009. Cell type specificity of PI3K signaling in Pdk1- and Pten-deficient brains. *Genes Dev* 23:1619–1624. <http://dx.doi.org/10.1101/gad.1799609>.
- Eickholt BJ, Ahmed AI, Davies M, Papakonstanti EA, Pearce W, Starkey ML, Bilancio A, Need AC, Smith AJ, Hall SM, Hamers FP, Giese KP, Bradbury EJ, Vanhaesebroeck B. 2007. Control of axonal growth and regeneration of sensory neurons by the p110 δ PI 3-kinase. *PLoS One* 2:e869. <http://dx.doi.org/10.1371/journal.pone.0000869>.
- Kwon CH, Luikart BW, Powell CM, Zhou J, Matheny SA, Zhang W, Li Y, Baker SJ, Parada LF. 2006. Pten regulates neuronal arborization and social interaction in mice. *Neuron* 50:377–388. <http://dx.doi.org/10.1016/j.neuron.2006.03.023>.
- Tohda C, Nakanishi R, Kadowaki M. 2009. Hyperactivity, memory deficit and anxiety-related behaviors in mice lacking the p85 α subunit of phosphoinositide-3 kinase. *Brain Dev* 31:69–74. <http://dx.doi.org/10.1016/j.braindev.2008.04.006>.
- Emamian ES, Hall D, Birnbaum MJ, Karayiorgou M, Gogos JA. 2004. Convergent evidence for impaired AKT1-GSK3 β signaling in schizophrenia. *Nat Genet* 36:131–137. <http://dx.doi.org/10.1038/ng1296>.
- Guo AY, Sun J, Riley BP, Thiselton DL, Kendler KS, Zhao Z. 2009. The dystrobrevin-binding protein 1 gene: features and networks. *Mol Psychiatry* 14:18–29. <http://dx.doi.org/10.1038/mp.2008.88>.
- Chubb JE, Bradshaw NJ, Soares DC, Porteous DJ, Millar JK. 2008. The DISC locus in psychiatric illness. *Mol Psychiatry* 13:36–64. <http://dx.doi.org/10.1038/sj.mp.4002106>.
- Butler MG, Dasouki MJ, Zhou XP, Talebizadeh Z, Brown M, Takahashi TN, Miles JH, Wang CH, Stratton R, Pilarski R, Eng C. 2005. Subset of individuals with autism spectrum disorders and extreme macrocephaly associated with germline PTEN tumour suppressor gene mutations. *J Med Genet* 42:318–321. <http://dx.doi.org/10.1136/jmg.2004.024646>.
- Zhou J, Parada LF. 2012. PTEN signaling in autism spectrum disorders. *Curr Opin Neurobiol* 22:873–879. <http://dx.doi.org/10.1016/j.comb.2012.05.004>.
- Alessi DR, James SR, Downes CP, Holmes AB, Gaffney PR, Reese CB, Cohen P. 1997. Characterization of a 3-phosphoinositide-dependent protein kinase which phosphorylates and activates protein kinase Balpa. *Curr Biol* 7:261–269. [http://dx.doi.org/10.1016/S0960-9822\(06\)00122-9](http://dx.doi.org/10.1016/S0960-9822(06)00122-9).
- Bayascas JR. 2010. PDK1: the major transducer of PI 3-kinase actions. *Curr Top Microbiol Immunol* 346:9–29.
- Pearce LR, Komander D, Alessi DR. 2010. The nuts and bolts of AGC protein kinases. *Nat Rev Mol Cell Biol* 11:9–22. <http://dx.doi.org/10.1038/nrm2822>.
- Biondi RM, Komander D, Thomas CC, Lizcano JM, Deak M, Alessi DR, Van Aalten DM. 2002. High resolution crystal structure of the human PDK1 catalytic domain defines the regulatory phosphopeptide docking site. *EMBO J* 21:4219–4228. <http://dx.doi.org/10.1093/emboj/cdf437>.
- Frodin M, Antal TL, Dummmler BA, Jensen CJ, Deak M, Gammeltoft S, Biondi RM. 2002. A phosphoserine/threonine-binding pocket in AGC kinases and PDK1 mediates activation by hydrophobic motif phosphorylation. *EMBO J* 21:5396–5407. <http://dx.doi.org/10.1093/emboj/cdf551>.
- Bayascas JR. 2008. Dissecting the role of the 3-phosphoinositide-dependent protein kinase-1 (PDK1) signalling pathways. *Cell Cycle* 7:2978–2982. <http://dx.doi.org/10.4161/cc.7.19.6810>.
- Zurashvili T, Cordon-Barris L, Ruiz-Babot G, Zhou X, Lizcano JM, Gomez N, Gimenez-Llort L, Bayascas JR. 2013. Interaction of PDK1 with phosphoinositides is essential for neuronal differentiation but dispensable for neuronal survival. *Mol Cell Biol* 33:1027–1040. <http://dx.doi.org/10.1128/MCB.01052-12>.
- Collins BJ, Deak M, Arthur JS, Armit LJ, Alessi DR. 2003. In vivo role of the PIF-binding docking site of PDK1 defined by knock-in mutation. *EMBO J* 22:4202–4211. <http://dx.doi.org/10.1093/emboj/cdg407>.
- Tronche F, Kellendonk C, Kretz O, Gass P, Anlag K, Orban PC, Bock R, Klein R, Schutz G. 1999. Disruption of the glucocorticoid receptor gene in the nervous system results in reduced anxiety. *Nat Genet* 23:99–103. <http://dx.doi.org/10.1038/12703>.
- Bayascas JR, Sakamoto K, Armit LJ, Arthur JS, Alessi DR. 2006. Evaluation of approaches to generation of tissue-specific knock-in mice. *J Biol Chem* 281:28772–28781. <http://dx.doi.org/10.1074/jbc.M606789200>.
- Kilkenny C, Browne WJ, Cuthill IC, Emerson M, Altman DG. 2010. Improving bioscience research reporting: the ARRIVE guidelines for reporting animal research. *J Pharmacol Pharmacother* 1:94–99. <http://dx.doi.org/10.4103/0976-500X.72351>.
- Gundersen HJ, Jensen EB. 1987. The efficiency of systematic sampling in stereology and its prediction. *J Microsc* 147:229–263. <http://dx.doi.org/10.1111/j.1365-2818.1987.tb02837.x>.
- Gimenez-Llort L, Fernandez-Teruel A, Escorihuela RM, Fredholm BB, Tobena A, Pekny M, Johansson B. 2002. Mice lacking the adenosine A1 receptor are anxious and aggressive, but are normal learners with reduced muscle strength and survival rate. *Eur J Neurosci* 16:547–550. <http://dx.doi.org/10.1046/j.1460-9568.2002.02122.x>.
- Rogers DC, Fisher EM, Brown SD, Peters J, Hunter AJ, Martin JE. 1997. Behavioral and functional analysis of mouse phenotype: SHIRPA, a proposed protocol for comprehensive phenotype assessment. *Mamm Genome* 8:711–713. <http://dx.doi.org/10.1007/s003539900551>.
- Torres-Lista V, Gimenez-Llort L. 2013. Impairment of nesting behaviour in 3xTg-AD mice. *Behav Brain Res* 247:153–157. <http://dx.doi.org/10.1016/j.bbr.2013.03.021>.
- García-Mesa Y, Lopez-Ramos JC, Gimenez-Llort L, Revilla S, Guerra R, Gruart A, LaFerla FM, Cristofol R, Gado Garcia JM, Sanfeliu C. 2011. Physical exercise protects against Alzheimer's disease in 3xTg-AD mice. *J Alzheimers Dis* 24:421–454. <http://dx.doi.org/10.3233/JAD-2011-101635>.
- Balendran A, Casamayor A, Deak M, Paterson A, Gaffney P, Currie R, Downes CP, Alessi DR. 1999. PDK1 acquires PDK2 activity in the presence of a synthetic peptide derived from the carboxyl terminus of PRK2. *Curr Biol* 9:393–404. [http://dx.doi.org/10.1016/S0960-9822\(99\)80186-9](http://dx.doi.org/10.1016/S0960-9822(99)80186-9).
- Biondi RM, Cheung PC, Casamayor A, Deak M, Currie RA, Alessi DR. 2000. Identification of a pocket in the PDK1 kinase domain that interacts

- with PIF and the C-terminal residues of PKA. *EMBO J* 19:979–988. <http://dx.doi.org/10.1093/emboj/19.5.979>.
34. Anjum R, Blenis J. 2008. The RSK family of kinases: emerging roles in cellular signalling. *Nat Rev Mol Cell Biol* 9:747–758. <http://dx.doi.org/10.1038/nrm2509>.
 35. Garcia-Martinez JM, Alessi DR. 2008. mTOR complex 2 (mTORC2) controls hydrophobic motif phosphorylation and activation of serum- and glucocorticoid-induced protein kinase 1 (SGK1). *Biochem J* 416:375–385. <http://dx.doi.org/10.1042/BJ20081668>.
 36. Balendran A, Hare GR, Kieloch A, Williams MR, Alessi DR. 2000. Further evidence that 3-phosphoinositide-dependent protein kinase-1 (PDK1) is required for the stability and phosphorylation of protein kinase C (PKC) isoforms. *FEBS Lett* 484:217–223. [http://dx.doi.org/10.1016/S0014-5793\(00\)02162-1](http://dx.doi.org/10.1016/S0014-5793(00)02162-1).
 37. Kharebava G, Makonchuk D, Kalita KB, Zheng JJ, Hetman M. 2008. Requirement of 3-phosphoinositide-dependent protein kinase-1 for BDNF-mediated neuronal survival. *J Neurosci* 28:11409–11420. <http://dx.doi.org/10.1523/JNEUROSCI.2135-08.2008>.
 38. Waite K, Eickholt BJ. 2010. The neurodevelopmental implications of PI3K signaling. *Curr Top Microbiol Immunol* 346:245–265. http://dx.doi.org/10.1007/82_2010_82.
 39. Jossin Y, Goffinet AM. 2007. Reelin signals through phosphatidylinositol 3-kinase and Akt to control cortical development and through mTOR to regulate dendritic growth. *Mol Cell Biol* 27:7113–7124. <http://dx.doi.org/10.1128/MCB.00928-07>.
 40. McManus EJ, Collins BJ, Ashby PR, Prescott AR, Murray-Tait V, Armit LJ, Arthur JS, Alessi DR. 2004. The in vivo role of PtdIns(3,4,5)P₃ binding to PDK1 PH domain defined by knockin mutation. *EMBO J* 23:2071–2082. <http://dx.doi.org/10.1038/sj.emboj.7600218>.
 41. Arencibia JM, Pastor-Flores D, Bauer AF, Schulze JO, Biondi RM. 2013. AGC protein kinases: From structural mechanism of regulation to allosteric drug development for the treatment of human diseases. *Biochim Biophys Acta* 1834:1302–1321. <http://dx.doi.org/10.1016/j.bbapap.2013.03.010>.
 42. Najafav A, Shpiro N, Alessi DR. 2012. Akt is efficiently activated by PIF-pocket- and PtdIns(3,4,5)P₃-dependent mechanisms leading to resistance to PDK1 inhibitors. *Biochem J* 448:285–295. <http://dx.doi.org/10.1042/BJ20121287>.
 43. Zhou X, Cordon-Barris L, Zurashvili T, Bayasas JR. 2014. Fine-tuning the intensity of the PKB/Akt signal enables diverse physiological responses. *Cell Cycle* 13:3164–3168. <http://dx.doi.org/10.4161/15384101.2014.962954>.
 44. Hauge C, Antal TL, Hirschberg D, Doehn U, Thorup K, Idrissova L, Hansen K, Jensen ON, Jorgensen TJ, Biondi RM, Frodin M. 2007. Mechanism for activation of the growth factor-activated AGC kinases by turn motif phosphorylation. *EMBO J* 26:2251–2261. <http://dx.doi.org/10.1038/sj.emboj.7601682>.
 45. Le Good JA, Ziegler WH, Parekh DB, Alessi DR, Cohen P, Parker PJ. 1998. Protein kinase C isoforms controlled by phosphoinositide 3-kinase through the protein kinase PDK1. *Science* 281:2042–2045. <http://dx.doi.org/10.1126/science.281.5385.2042>.
 46. Dutil EM, Tokar A, Newton AC. 1998. Regulation of conventional protein kinase C isozymes by phosphoinositide-dependent kinase 1 (PDK-1). *Curr Biol* 8:1366–1375. [http://dx.doi.org/10.1016/S0960-9822\(98\)00017-7](http://dx.doi.org/10.1016/S0960-9822(98)00017-7).
 47. Datta SR, Brunet A, Greenberg ME. 1999. Cellular survival: a play in three Akts. *Genes Dev* 13:2905–2927. <http://dx.doi.org/10.1101/gad.13.22.2905>.
 48. Yoshimura T, Arimura N, Kawano Y, Kawabata S, Wang S, Kaibuchi K. 2006. Ras regulates neuronal polarity via the PI3-kinase/Akt/GSK-3beta/CRMP-2 pathway. *Biochem Biophys Res Commun* 340:62–68. <http://dx.doi.org/10.1016/j.bbrc.2005.11.147>.
 49. Kishi M, Pan YA, Crump JG, Sanes JR. 2005. Mammalian SAD kinases are required for neuronal polarization. *Science* 307:929–932. <http://dx.doi.org/10.1126/science.1107403>.
 50. Barnes AP, Lilley BN, Pan YA, Plummer LJ, Powell AW, Raines AN, Sanes JR, Polleux F. 2007. LKB1 and SAD kinases define a pathway required for the polarization of cortical neurons. *Cell* 129:549–563. <http://dx.doi.org/10.1016/j.cell.2007.03.025>.
 51. Laguesse S, Creppe C, Nedialkova DD, Prevot PP, Borgs L, Huysseune S, Franco B, Duysens G, Krusy N, Lee G, Thelen N, Thiry M, Close P, Chariot A, Malgrange B, Leidel SA, Godin JD, Nguyen L. 2015. A dynamic unfolded protein response contributes to the control of cortical neurogenesis. *Dev Cell* 35:553–567. <http://dx.doi.org/10.1016/j.devcel.2015.11.005>.
 52. Creppe C, Malinouskaya L, Volvert ML, Gillard M, Close P, Malaise O, Laguesse S, Cornez I, Rahmouni S, Ormenese S, Belachew S, Malgrange B, Chapelle JP, Siebenlist U, Moonen G, Chariot A, Nguyen L. 2009. Elongator controls the migration and differentiation of cortical neurons through acetylation of alpha-tubulin. *Cell* 136:551–564. <http://dx.doi.org/10.1016/j.cell.2008.11.043>.
 53. Holz MK, Ballif BA, Gygi SP, Blenis J. 2005. mTOR and S6K1 mediate assembly of the translation preinitiation complex through dynamic protein interchange and ordered phosphorylation events. *Cell* 123:569–580. <http://dx.doi.org/10.1016/j.cell.2005.10.024>.
 54. Magnuson B, Ekim B, Fingar DC. 2012. Regulation and function of ribosomal protein S6 kinase (S6K) within mTOR signalling networks. *Biochem J* 441:1–21. <http://dx.doi.org/10.1042/BJ20110892>.
 55. Selemo LD, Goldman-Rakic PS. 1999. The reduced neuropil hypothesis: a circuit based model of schizophrenia. *Biol Psychiatry* 45:17–25. [http://dx.doi.org/10.1016/S0006-3223\(98\)00281-9](http://dx.doi.org/10.1016/S0006-3223(98)00281-9).
 56. Selemo LD, Rajkowska G, Goldman-Rakic PS. 1998. Elevated neuronal density in prefrontal area 46 in brains from schizophrenic patients: application of a three-dimensional, stereologic counting method. *J Comp Neurol* 392:402–412.
 57. Akbarian S, Huang HS. 2006. Molecular and cellular mechanisms of altered GAD1/GAD67 expression in schizophrenia and related disorders. *Brain Res Rev* 52:293–304. <http://dx.doi.org/10.1016/j.brainresrev.2006.04.001>.
 58. Lewis DA, Curley AA, Glausier JR, Volk DW. 2012. Cortical parvalbumin interneurons and cognitive dysfunction in schizophrenia. *Trends Neurosci* 35:57–67. <http://dx.doi.org/10.1016/j.tins.2011.10.004>.
 59. Miyamoto Y, Nitta A. 2014. Behavioral phenotypes for negative symptoms in animal models of schizophrenia. *J Pharmacol Sci* 126:310–320. <http://dx.doi.org/10.1254/jphs.14R02CR>.
 60. Stefansson H, Sigurdsson E, Steinthorsdottir V, Bjornsdottir S, Sigmundsson T, Ghosh S, Brynjolfsson J, Gunnarsdottir S, Ivarsson O, Chou TT, Hjaltason O, Birgisdottir B, Jonsson H, Gudnadottir VG, Gudmundsdottir E, Bjornsson A, Ingvarsson B, Ingason A, Sigfusson S, Hardardottir H, Harvey RP, Lai D, Zhou M, Brunner D, Mutel V, Gonzalo A, Lemke G, Sainz J, Johannesson G, Andresson T, Gudbjartsson D, Manolescu A, Frigge ML, Gurney ME, Kong A, Gulcher JR, Petursson H, Stefansson K. 2002. Neuregulin 1 and susceptibility to schizophrenia. *Am J Hum Genet* 71:877–892. <http://dx.doi.org/10.1086/342734>.
 61. Tosato S, Dazzan P, Collier D. 2005. Association between the neuregulin 1 gene and schizophrenia: a systematic review. *Schizophr Bull* 31:613–617. <http://dx.doi.org/10.1093/schbul/sbi043>.